UNIVERSITY OF HELSINKI REPORT SERIES IN PHYSICS

HU-P-D184

DISORDERED MATTER STUDIED BY X-RAY RAMAN SCATTERING

Tuomas Pylkkänen

Department of Physics
Faculty of Science
University of Helsinki
Helsinki, Finland

ACADEMIC DISSERTATION

To be presented, with the permission of
the Faculty of Science of the University of Helsinki,
for public criticism in Auditorium E204
of the Department of Physics (Physicum),
Gustaf Hällströmin katu 2a, on 11 August 2011 at 12:15.

Helsinki 2011

Supervisors:

Prof. Keijo Hämäläinen
Department of Physics
University of Helsinki
Helsinki, Finland

Dr. Simo Huotari
Department of Physics
University of Helsinki
Helsinki, Finland

Dr. Giulio Monaco
European Synchrotron Radiation Facility
Grenoble, France

Pre-examiners:

Prof. Abhay Shukla
Université Pierre et Marie Curie- Paris 6
Paris, France

Dr. Christian Sternemann
Technische Universität Dortmund
Dortmund, Germany

Opponent:

Dr. Uwe Bergmann
Linac Coherent Light Source
SLAC National Accelerator Laboratory
Menlo Park, CA, USA

Custos:

Prof. Keijo Hämäläinen
Department of Physics
University of Helsinki
Helsinki, Finland

Report Series in Physics HU-P-D184
ISSN 0356-0961
ISBN 978-952-10-6885-0 (printed version)
ISBN 978-952-10-6886-7 (pdf version)
http://ethesis.helsinki.fi/
Helsinki University Print
Helsinki 2011

Preface

The work presented in this thesis was performed at the Department of Physics of the University of Helsinki and the European Synchrotron Radiation Facility (ESRF) in Grenoble, France. I wish to thank Prof. Juhani Keinonen for the opportunity to work at the Department of Physics, and the Academy of Finland, the ESRF, the Magnus Ehrnrooth Foundation, and the Emil Aaltonen Foundation for funding.

I had the pleasure of collaborating with a large group of people whose help and influence cannot be understated. Above all, I benefited from having three expert supervisors. I am indebted to Prof. Keijo Hämäläinen for introducing me to x-ray physics and guiding me throughout my studies. Keijo has an infectious enthusiasm for physics, and I could always count on him for sound advise on both work and personal matters. Second, I wish to thank Dr. Giulio Monaco for guidance especially during my time at the ESRF. I was deeply impressed by Giulio's laser-like focus and relentless inquisitiveness, and remain thankful for the time he found for discussions among his busy schedule. Third, I wish to thank Dr. Simo Huotari for his exceptional advice and infinite patience. Simo taught me everything practical—and practically everything—that I learned about synchrotron science. He also went to great lengths to welcome me and help me get the most out of the unique experience of working in Grenoble.

The staff of the "x-ray lab" at the Department of Physics is fondly acknowledged for their company during these years, from the daily coffee breaks to the weekly floorball matches and the occasional parties. I wish to thank everyone in Keijo's group and in particular my co-authors for their important contributions: Dr. Mikko Hakala, Dr. Aleksi Soininen, Arto Sakko, and Jussi Lehtola. I am also grateful of Arto, Mikko, and Dr. Szabolcs Galambosi for indulging in the arguably non-productive yet very rewarding discussions on the nature of photons, electrons and various physical phenomena.

The three years spent in Grenoble formed the basis of the thesis, but were also extremely rewarding personally. I wish to thank the staff of beamline ID16 for a unique working atmosphere and all the contributions to the work. In particular, the work benefited from the analyzer-making expertise of Dr. Roberto Verbeni, the high-pressure magic of Dr. Valentina Giordano, and the expert technical skills of Christian Henriquet who saved the day on a number of occasions. The sample environment and detector specialists of the ESRF are also gratefully acknowledged. The daily grind of the PhD project would have been infinitely more boring without the company of Drs. Beatrice Ruta, Laura Simonelli, Giacomo Baldi, and György Vankó. Finally, a thesis is not only a result of successful projects, but also of trials, failures, and dead ends. I learned a lot from projects with i.a. Drs. Wilson Crichton and Daniel Bowron.

A most memorable aspect of the whole endeavor is meeting new people at the melting pot of the Polygone Scientifique. I am overwhelmed by the number of persons I would like to thank for sharing the good times and the bad, from the heights of La

Dent de Crolles to the depths of Le Vieux Manoir. Simo and Liisa kept a welcoming house which was also the focal point of the Finnish community (with Manu, Nina, and Heikki). I will always remember the warm welcome to the Italian community by Bea, Vale (×2), Laura, Giacomo, and countless others. I enjoyed tremendously the Spanish influence of Javier (×2), Willy, Félix, Yolanda, Sergio, Jonan, Roberto, Manu... I would also like thank the Alsace-Lorraine crew for their hospitality, Moritz for delightful dinners, and the fun-loving Frenchmen Séb and Raph for showing me that the French can rock.

I remain grateful for all my friends back in Finland for their fellowship and welcome distractions during my studies. I'm particularly happy of your memorable visits to Grenoble, keeping in touch during my absence, and welcoming me back.

Since my childhood and throughout my studies my parents and sisters have encouraged my curiosity for the natural world. Your conscious support and perhaps unconscious influence have given me the confidence and tenacity that was often necessary for pursuing this goal. Finally, words are not enough to thank Kristiina for her endless patience and loving encouragement.

T. Pylkkänen: Disordered matter studied by x-ray Raman scattering, University of Helsinki, 2011, 46 pages + appendices. University of Helsinki, Report Series in Physics, HU-P-D184.

Classification (INSPEC): A3520G, A6110F, A6125E, A7115M, A7125M, A7870C
Keywords: inelastic x-ray scattering, x-ray Raman scattering, synchrotron radiation, disordered matter, density of states, hydrogen bonding, molecular liquids, water

Abstract

Spectroscopy can provide valuable information on the structure of disordered matter beyond that which is available through e.g. x-ray and neutron diffraction. X-ray Raman scattering is a non-resonant element-sensitive process which allows bulk-sensitive measurements of core-excited spectra from light-element samples. In this thesis, x-ray Raman scattering is used to study the local structure of hydrogen-bonded liquids and solids, including liquid water, a series of linear and branched alcohols, and high-pressure ice phases.

Connecting the spectral features to the local atomic-scale structure involves theoretical references, and in the case of hydrogen-bonded systems the interpretation of the spectra is currently actively debated. The systematic studies of the intra- and intermolecular effects in alcohols, non-hydrogen-bonded neighbors in high-pressure ices, and the effect of temperature in liquid water are used to demonstrate different aspects of the local structure that can influence the near-edge spectra. Additionally, the determination of the extended x-ray absorption fine structure is addressed in a momentum-transfer dependent study. This work demonstrates the potential of x-ray Raman scattering for unique studies of the local structure of a variety of disordered light-element systems.

List of papers

This thesis consists of an introductory part and five research articles, which are referred to by the Roman numerals **I**–**V** throughout the text.

I Roberto Verbeni, **Tuomas Pylkkänen**, Simo Huotari, Laura Simonelli, György Vankó, Keith Martel, Christian Henriquet and Giulio Monaco. *Multiple-element spectrometer for non-resonant inelastic x-ray spectroscopy of electronic excitations.*
Journal of Synchrotron Radiation **16**, 469 (2009).

II **Tuomas Pylkkänen**, Jussi Lehtola, Mikko Hakala, Arto Sakko, Giulio Monaco, Simo Huotari, and Keijo Hämäläinen. *Universal signature of hydrogen bonding in the oxygen K-edge spectrum of alcohols.*
The Journal of Physical Chemistry B **114**, 13076 (2010).

III **Tuomas Pylkkänen**, Valentina M. Giordano, Jean-Claude Chervin, Arto Sakko, Mikko Hakala, J. Aleksi Soininen, Keijo Hämäläinen, Giulio Monaco, and Simo Huotari. *Role of non-hydrogen-bonded molecules in the oxygen K-edge spectrum of ice.*
The Journal of Physical Chemistry B **114**, 3804 (2010).

IV **Tuomas Pylkkänen**, Arto Sakko, Mikko Hakala, Keijo Hämäläinen, Giulio Monaco, and Simo Huotari. *Temperature dependence of the near-edge spectrum of water.*
Submitted to The Journal of Physical Chemistry B (2011).

V Simo Huotari, **Tuomas Pylkkänen**, J. Aleksi Soininen, Joshua Kas, Keijo Hämäläinen, and Giulio Monaco. *X-ray Raman scattering based EXAFS beyond the dipole limit.*
Submitted to the Journal of Synchrotron Radiation (2011).

Author's contribution

The author of this thesis is the principal author of papers **II**–**IV** and a contributing author to papers **I** and **V**. He has planned, performed, and analyzed the results from the x-ray Raman scattering experiments in the papers. He has performed the DFT calculations of papers **III**–**IV** and the RSMS calculations of papers **II**–**IV**, and analyzed the computational results in papers **II** and **V**. The author has had an active role in the interpretation of the results and the writing of the papers.

Contents

1 Introduction **1**

2 Structure of disordered matter **1**
2.1 Typical methods for studying local structure 2
2.2 X-ray spectroscopies and disordered matter 4

3 Inelastic x-ray scattering **6**
3.1 Interaction of x-rays with matter 6
3.2 Non-resonant inelastic x-ray scattering 7
3.3 X-ray Raman scattering 9

4 Experimental methods **10**
4.1 Synchrotron radiation spectroscopy 10
4.2 Data analysis 11
4.3 Sample environments 13
4.3.1 Flow cell for liquid samples 13
4.3.2 High-pressure studies with a diamond anvil cell 14

5 Computational methods **15**
5.1 Near-edge spectra with density-functional theory 15
5.2 Atomic background and momentum transfer dependence 17
5.3 Extended fine structure with real-space multiple-scattering approach . . 19

6 Summary of papers **20**
6.1 Paper I: Multiple-element spectrometer for non-resonant inelastic x-ray spectroscopy of electronic excitations 20
6.2 Paper II: Universal signature of hydrogen bonding at the oxygen K-edge of alcohols 21
6.3 Paper III: Role of non-hydrogen-bonded molecules in the oxygen K-edge spectrum of ice 21
6.4 Paper IV: Temperature dependence of the near-edge spectrum of water 22
6.5 Paper V: X-ray Raman scattering based EXAFS beyond the dipole limit 23

7 Concluding remarks **24**

References **27**

1 Introduction

Describing the macroscopic properties of matter beginning from the atomic-scale structures and interactions is one of the fundamental goals of condensed matter physics. Much of the progress in the field stems from understanding and controlling the electronic properties of crystalline materials. Disordered matter—such as liquids and amorphous materials—is much less understood. Despite the lack of long-range order in disordered matter, there often exists a pronounced *local* structure at the atomic and molecular level. However, it is usually difficult to access this local structure since much of it is averaged out over the time and length scales typically accessible to experiments.

In this thesis a novel synchrotron radiation-based spectroscopic method has been applied to study the structure of disordered matter. X-ray Raman scattering (XRS) is an element-specific method for probing unoccupied electronic states, in particular those related to intermolecular bonds. XRS allows experimental studies of the local structure of matter via the spectral signatures due to bond formation and bonding changes. It is thus an indirect structural probe, similar to many established methods such as infrared vibrational and nuclear magnetic resonance spectroscopy. Such indirect probes can add crucial information on the local structure that is not otherwise accessible.

The main applications in this thesis are hydrogen-bonded liquids and solids, which are currently actively studied with various x-ray spectroscopies [1–8]. One fundamental subject of interest is the local structure of liquid water, which is constantly discussed even after decades of intense study [9–11]. Interpreting the new spectroscopic results has led to controversial discussions on e.g. the nature of the hydrogen bond [1, 12, 13] and the degree of hydrogen bonding in liquid water [2, 3, 14]. Making the new results compatible with previous studies requires both careful analysis and critical re-evaluation of previous results.

In the introductory part of the thesis the background of the work is discussed, starting with the structure of disordered matter, followed by a short review of inelastic x-ray scattering and XRS. The experimental and computational methods are described briefly in the ensuing sections. Finally, the background and main results of the papers are summarized.

2 Structure of disordered matter

In terms of structure, condensed matter can be broadly divided into ordered and disordered matter. The former is easy to define as the perfect periodic order of idealized crystals. Disorder is less clearly defined [15] and may be thought to develop in stages: from perfect crystalline to polycrystalline to amorphous (non-crystalline solid) and liquid matter.

Even though long-range order is lost in liquids, there often exists a pronounced local

structure that correlates atomic densities over several intermolecular distances. Even the most simple model, the hard-sphere liquid, has clear local structure as evidenced by the pair correlation function [15–18]. This structure, stemming only from a repulsive interaction between the spheres, is a good approximation for the local structure of non-associating liquids (e.g. liquid argon). Liquids that have more complex intermolecular interactions may have quite elaborate local structure that fundamentally influences their microscopic and macroscopic properties.

Liquid water is such a system. In addition to the repulsive interactions there are complex attractive interactions in the form of hydrogen bonds (HBs) [19]. The combination of directionality and relative weakness of the HB (5.5 kcal/mol per bond in ice [10], corresponding to $\sim 9 k_B T$ at 300 K) yields complex transient local structures. In water HBs are conventionally thought to form a continuous distorted network with similarities to the local structure of ice phases [9–11]. This HB network fundamentally influences the macroscopical properties of liquid water which differ tremendously from simple hard-sphere-like liquids. In particular, many of the thermodynamical response functions have non-linear behavior and various extrema in the stable temperature region at ambient pressure, and even exhibit apparent divergences in the supercooled region [20–22]. Furthermore, the properties of liquid water are strongly influenced by solutes (e.g. ions [23]) and confinement (in particular at biological interfaces [24]). Water is thus both a model system of H-bonding and a very interesting subject in its own right. In the following established methods for the study of the local structure of disordered matter are introduced and their application to liquid water is presented.

2.1 Typical methods for studying local structure

X-ray and neutron diffraction probe the static density correlations of electrons and nuclei, respectively. In crystalline matter diffraction leads to Bragg reflections which can be used to map the reciprocal lattice and, in principle, to fully solve the structure of the sample under study. In liquid and amorphous matter, the loss of long-range order limits the information available through diffraction to the radial distribution function $g(r)$. Neutron diffraction with isotopic substitution and anomalous x-ray diffraction enable the determination of partial radial distribution functions, e.g. the pairwise components $g_{\mathrm{OO}}(r)$, $g_{\mathrm{OH}}(r)$, and $g_{\mathrm{HH}}(r)$ in the case of H_2O. However, higher-order correlation functions (including angular dependencies) cannot be directly accessed. Neutron diffraction is, by definition, only sensitive to the positions of the nuclei, but also x-ray diffraction is inherently more sensitive to the spatially concentrated core electrons than the spatially extended valence electrons, which further hides details of bonding.

A number of computational techniques have been introduced to maximally utilize the limited structural data available through diffraction. The most sophisticated are

reverse-Monte Carlo techniques [25, 26] which can incorporate further physical considerations in the form of pair potentials which disfavor high-energy structures [27, 28]. The application of these methods to liquid water, however, has shown diffraction to be rather insensitive to the details of H-bonding. Diffraction data can be made consistent both with traditional near-tetrahedral structural models [14, 29], and the recently introduced asymmetric structural models, which impose a high level of broken HBs [27, 30]. The implications of such asymmetic models for other measurables are actively debated [11, 14, 31–33].

Molecular-dynamics (MD) simulations can offer a complete description of the local structure and dynamics of disordered matter and have contributed vastly to our understanding of the subject [34, 35]. Modeling the interactions between atoms and molecules, however, is a complex problem in itself and requires much input in the form of microscopic and macroscopic properties that can be compared with the predictions from simulations. Classical MD simulations typically utilize pair potentials to model all interactions between the simulated molecules, which may be rigid or flexible. The pair potentials are parametrized based on model calculations or in order to reproduce selected macroscopic properties. Classical MD is a very developed field; for liquid water, more than 50 potentials have been parametrized [36]. There are extraordinary achievements such as modeling the polymorphic phase diagram of ices [37] and reproducing some of the anomalous thermodynamical properties of the liquid [38]. However, one fundamental issue remains: classical MD simulations of liquid water typically have little predictive power beyond that behavior which they have been fitted to reproduce [36]. Depending on the choice of properties that a model is imposed to reproduce, the local structures produced by the simulations may differ dramatically [27, 30, 36].

Parameter-free approaches such as *ab initio* molecular dynamics (AIMD) which seek to model the intermolecular interactions with quantum chemistry calculations promise to overcome this limitation [39]. However, they are computationally very expensive and limited to small periodic systems of a few dozen molecules and thus may be influenced by size effects and limited simulation time. For most applications classical MD simulations remain the only practical approach. As mentioned above, diffraction data is often not sensitive enough to the details of bonding to discriminate e.g. between the structures produced by different classical MD water models. It is therefore very important to offer structural information beyond the $g(r)$ to reliably constrain (or expand) the range of possible local structures in disordered matter.

Spectroscopy is a powerful alternative method for obtaining structural information. There is often a connection between the local structure and an electronic, vibrational, or nuclear spin excitation. In this way, spectroscopic methods are indirect structural probes that can add complementary information about the local structure in terms of e.g. chemical bonding. Examples of widely used spectroscopic tools include

infrared/Raman vibrational spectroscopy and nuclear magnetic resonance (NMR) spectroscopy [40]. In the case of liquid water, the most studied vibrational excitation is the intramolecular OH stretch vibration which is sensitive to the HB enviroment [41–43]. The field is highly developed with applications such as pump-and-probe spectroscopy allowing time-dependent effects like HB lifetimes to be studied [43–45]. NMR spectroscopy has been used to e.g. derive temperature-dependent HB distributions [46].

In comparing results from different techniques it is important to be aware of the relevant time and length scales probed by each technique [9]. For example, x-ray diffraction probes the diffusionally-averaged structure, while IR/Raman spectroscopy probes the vibrationally-averaged structure (timescale $\lesssim 10^{-12}$ s), and the x-ray spectroscopies presented below probe the instantaneous structure (timescale $\lesssim 10^{-15}$ s). Liquids such as water may appear completely different at various timescales as separate degrees of freedom are frozen out at specific timescales [9, 15].

2.2 X-ray spectroscopies and disordered matter

Recently various x-ray spectroscopies have been applied to the study of disordered matter and in particular liquid water. The common factor among these techniques (inelastic x-ray scattering, x-ray absorption, and x-ray emission) is that they probe electronic transitions.

Compton scattering (CS) provides information on the ground-state electron momentum density and is thus complementary to x-ray diffraction. Chemical bonding induces an oscillatory signal in the Compton profile which can be measured to a high accuracy [47]. Recently, CS has been applied to study e.g. the HB in water [48–51], ice [1, 5, 12, 52–54], aqueous solutions [55], alcohol isomers [56], and clathrate hydrates [57, 58].

X-ray absorption spectroscopy (XAS) and x-ray Raman scattering (XRS)—the subject of this thesis—probe the unoccupied electronic states via core-electron excitation (Sec. 3.1). In XAS the final states are accessed by resonant absorption, while in XRS they are reached by a non-resonant photon-in–photon-out process. It is customary to divide the spectrum into two regions: the near-edge structure (XANES) and the extended x-ray absorption fine structure (EXAFS), since their interpretation is different. The EXAFS region exhibits an oscillatory signal due to scattering of the photoelectron from nearest neighbors. The Fourier transform of the EXAFS signal is an effective radial-distribution function, although various effects beyond the density correlations contribute to the signal. EXAFS has become a routine technique for the study of local structure in disordered matter [59–62].

The near-edge region is naturally described in terms of unoccupied electronic states. In the absence of periodicity and band structure this is well described by molecular orbitals. The lowest unoccupied states include anti-bonding orbitals related to chem-

ical bonds. XAS and XRS are thus explicitly sensitive to chemical bonding, although connecting spectral features with structure in general requires electronic structure calculations. X-ray emission spectroscopy (XES) probes the occupied electronic states of a core-excited atom via the x-rays emitted as the core hole decays. It is consequently very sensitive to valence electron states [6, 8], although various dynamical effects may also influence the spectra [8, 63].

XAS and XRS are becoming standard tools for studying local structure in a variety of systems. In the following some recent applications of XRS are presented. These studies are essentially similar to XAS studies (e.g. Refs. 64, 65), but they exploit the non-resonant character of the XRS process, which allows hard-x-ray studies of soft-x-ray absorption edges. Low-Z elements can thus be studied in a bulk-sensitive manner or embedded in a sample environment for e.g. high-pressure studies [66]. Due to the indirect connection of the spectrum and local structure most approaches fall into two categories: (a) interpreting the spectra in terms of empirical references or "fingerprints", and (b) comparing the results to computations of the electronic structure of MD snapshots or model clusters.

Notable examples of using experimental fingerprints include the studies of the local coordination and bonding changes under pressure: element-selective coordination changes in borate glasses [67–69] and SiO_2 glass [70]; and hybridization changes in compressed superhard graphite [71], boron nitride [72], C_{60} fullerenes and multi-wall carbon nanotubes [73], and benzene [74]. Other studies include an analysis of the aromaticity of carbon in asphaltene [75] and separating the contributions from side chains and backbone in an aligned polymer [76].

Electronic structure calculations have been used e.g. in the studies of charge transfer in Li-intercalated graphite [77], the local electronic structure of $C_2B_{10}H_{12}$ [78] and α-Li_3N [79], suboxide interfaces in amorphous SiO [80], and hydrate formation THF clathrate [81]. One particularly active field of study has been H-bonding in water and ices [2,4,7,26,31,82–88]. The interpretation of the oxygen near-K-edge spectra in water vapor, liquid water, and in the bulk and surface of ice has led to intense debate. In particular, the failure of calculations to reproduce the measured liquid water spectrum using traditional structural models has led to the introduction of asymmetric structure models [2, 31, 89]. The reliability of the spectral calculations has been repeatedly challenged [90–94] and advanced [88, 89, 95, 96], while the implications of the asymmetric structure models to other observables are actively debated [6, 8, 14, 31, 33, 63]. In order to contribute to the discussion it is extremely useful to offer new experimental data that can be compared with calculations and serve as empirical fingerprints.

The work presented in this thesis utilizes many of these approaches. Paper **I** describes the experimental techniques used to measure XRS. In paper **II** the signal of H-bonding in alcohols is studied by combining experiments with spectral calculations of model clusters and MD snapshots. In paper **III** the spectra of high-pressure ices are

used as empirical references to study effects beyond H-bonding on the water spectrum. Spectral calculations are also used to confirm the validity of the results. In paper **IV** the energetics of the structural changes underlying the temperature dependence of the liquid water spectrum have been studied with an approach that is common in the analysis of vibrational spectroscopy. The EXAFS region—which has been exploited very little with XRS—is studied in detail in paper **V**.

3 Inelastic x-ray scattering

3.1 Interaction of x-rays with matter

X-rays interact with electrons through a variety of processes of which relevant for the current work are photoelectric absorption and non-resonant scattering (elastic and inelastic). Once the interaction processes are understood, absorption and scattering experiments can be used to probe the electronic structure and excitations in matter. The practical implications for applications follow from the special properties of each interaction process coupled with the advances and limitations of currently achievable instrumentation. In the following, a brief theoretical description of x-ray absorption and non-resonant x-ray scattering is given. Following the typical conventions of x-ray physics, atomic units are used ($\hbar = e = m_e = c\alpha = 1$), while energies are given in eV and distances in Å.

The non-relativistic cross-sections of absorption and scattering may be derived with perturbation theory from the photon-electron interaction Hamiltonian $\hat{H}_{\text{int}} = \mathbf{p}\cdot\mathbf{A} + \frac{1}{2}|\mathbf{A}|^2$, where $\mathbf{p}$ is the momentum of the electron and $\mathbf{A}$ the vector potential of the electromagnetic wave. [47,97,98] The transition rate from a given initial (photon + electron) state to a given final state can be obtained with Fermi's golden rule. As the quantized vector potential operator $\mathbf{A}$ is linear in the photon creation and annihilation operators, applying first-order perturbation theory on $\hat{H}_{\text{int}}$ yields absorption and emission from the term $\mathbf{p}\cdot\mathbf{A}$, and scattering from the term $|\mathbf{A}|^2$. Second-order perturbation of the $\mathbf{p}\cdot\mathbf{A}$ term involves intermediate states and yields resonant scattering, which is not considered in this work.

For x-ray absorption from an electronic state $|I\rangle$ to $|F\rangle$, Fermi's golden rule gives the transition rate [97, 99]

$$w_{I\to F} \propto \left|\langle F|e^{i\mathbf{k}_1\cdot\mathbf{r}}\,(\hat{\mathbf{e}}_1\cdot\mathbf{p})|I\rangle\right|^2 \delta(E_F - E_I - \omega_1), \tag{1}$$

where $\mathbf{r}$ is the electron position and ω_1 is the energy, $\hat{\mathbf{e}}_1$ the polarization vector, and $\mathbf{k}_1$ the wavevector of the incident photon. Within the dipole approximation $e^{i\mathbf{k}_1\cdot\mathbf{r}} \approx 1$ and, by transforming the momentum operator to the position operator, the cross section

becomes [97, 99]

$$\sigma_{\mathrm{XAS}}(\omega_1) \propto \omega_1 \sum_F \left|\langle F|\, \hat{\mathbf{e}}_1 \cdot \mathbf{r}|I\rangle\right|^2 \delta(E_F - E_I - \omega_1). \tag{2}$$

The x-ray absorption cross section is proportional to λr_0 [98], where r_0 is the classical electron radius and λ is the photon wavelength (for x-rays, $\lambda \gg r_0$).

3.2 Non-resonant inelastic x-ray scattering

When the energy ω_1 of an incident x-ray photon is far from any electronic transition energies, non-resonant inelastic x-ray scattering (NRIXS) may occur as depicted in Fig. 1: the photon is absorbed and another photon is emitted with energy ω_2 and momentum $\mathbf{k}_2$. The scattering process has transferred energy $\omega = \omega_1 - \omega_2$ and momentum $\mathbf{q} = \mathbf{k}_1 - \mathbf{k}_2$ to the electronic system, creating an excitation. The magnitude of the momentum transfer[1] is given by

$$q = \frac{1}{c}\sqrt{\omega_1^2 + \omega_2^2 - 2\omega_1\omega_2 \cos\phi}, \tag{3}$$

where ϕ is the scattering angle. By measuring the cross-section of the process in relevant ω and $\mathbf{q}$ ranges, one can map the electronic excitation spectrum of the system under study.

The transition rate for non-resonant scattering is [47, 97]

$$w_{I\to F} \propto \left|\langle F|\, \hat{\mathbf{e}}_1\, e^{i\mathbf{k}_1\cdot\mathbf{r}} \cdot \hat{\mathbf{e}}_2\, e^{-i\mathbf{k}_2\cdot\mathbf{r}}|I\rangle\right|^2 \delta(E_F - E_I - \omega). \tag{4}$$

This leads to the double-differential cross-section known as the non-resonant Kramers-Heisenberg formula [47]:

$$\frac{\mathrm{d}^2\sigma}{\mathrm{d}\Omega\, \mathrm{d}\omega} = r_0^2 \left(\frac{\omega_2}{\omega_1}\right) \sum_F \left|\langle F| \sum_j e^{i\mathbf{q}\cdot\mathbf{r}_j}|I\rangle (\hat{\mathbf{e}}_1 \cdot \hat{\mathbf{e}}_2)\right|^2 \delta(E_F - E_I - \omega), \tag{5}$$

where the sum over j is over all electrons (positions $\mathbf{r}_j$), and all transitions allowed by energy conservation are considered.

The cross-section can be separated into two factors. The first is the Thomson cross section that describes the photon-electron coupling and depends on the experimental arrangement through the photon energies ω_i and polarization vectors $\hat{\mathbf{e}}_i$:

$$\left(\frac{\mathrm{d}\sigma}{\mathrm{d}\Omega}\right)_{\mathrm{Th}} = r_0^2 \left(\frac{\omega_2}{\omega_1}\right) |\hat{\mathbf{e}}_1 \cdot \hat{\mathbf{e}}_2|^2. \tag{6}$$

The Thomson cross section is proportional to r_0^2, and non-resonant scattering is thus weak compared to absorption in the ∼10 keV range (apart from diffraction).

[1] The atomic unit (a.u.) of momentum is $\hbar/a_0$ (a_0 is the Bohr radius).

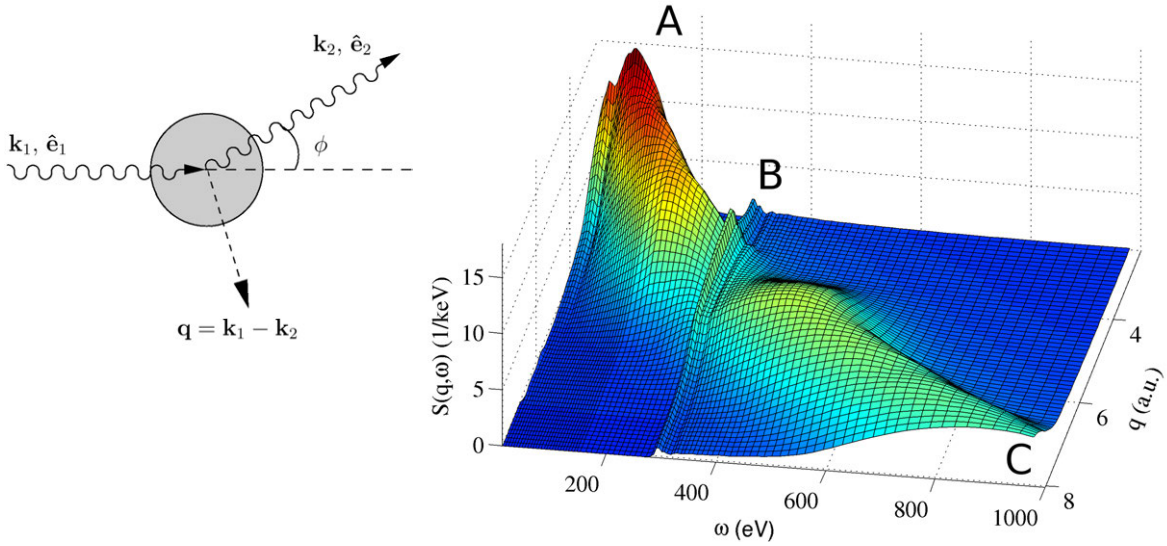

Figure 1: Left: Non-resonant scattering process. Right: Schematic dynamic structure factor $S(q,\omega)$ of polycrystalline diamond. Plasmons and other excitations (A) are visible at low q and ω, and the Compton profile (C) at large q and ω. The carbon K-edge (B) is at $\omega = 285$ eV.

The second factor is called the dynamic structure factor, and it contains all the material-dependent information accessible in a non-resonant scattering experiment:

$$S(\mathbf{q},\omega) = \sum_F \left|\langle F| \sum_j e^{i\mathbf{q}\cdot\mathbf{r}_j} |I\rangle\right|^2 \delta(E_F - E_I - \omega). \tag{7}$$

For elastic scattering, $|F\rangle = |I\rangle$ and $\omega = 0$. Then $S(\mathbf{q},\omega)$ reduces to $S(\mathbf{q})$ i.e. the static structure factor which is observed in x-ray diffraction.

The formulation of van Hove connects $S(\mathbf{q},\omega)$ to the self-correlation of the electron density $\rho(\mathbf{r},t)$ through a Fourier transform over space and time [47]

$$S(\mathbf{q},\omega) = \frac{1}{2\pi} \iint \mathrm{d}\mathbf{r}\, \mathrm{d}t\, e^{i(\mathbf{q}\cdot\mathbf{r}-\omega t)} \int \mathrm{d}\mathbf{r}' \left\langle \rho(\mathbf{r}'-\mathbf{r},t)\, \rho(\mathbf{r}',0) \right\rangle, \tag{8}$$

where the brackets denote the ground-state expectation value. Inverses of the momentum transfer q^{-1} and energy transfer ω^{-1} determine the length and time scales, respectively, over which the density correlations are studied. A schematic spectrum is shown in Fig. 1(b). Accessible excitations include a range of collective excitations (e.g. phonons and plasmons) at low energy transfers, inner-shell excitations at characteristic values of ω, and single-particle excitations (Compton scattering) at high energy and momentum transfers.

A large contribution to the $S(\mathbf{q},\omega)$ is given by plasmons [100], i.e. collective valence-electron excitations, which are prominent when $q \sim r_c^{-1}$ and $\omega \sim \omega_p$ (r_c is the interparticle separation and $\omega_p(q)$ the plasmon energy) [47]. The plasmon contribution disperses

and broadens with increasing q. At large momentum transfers, $q \gg r_c^{-1}$ and $\omega \gg E_B$ (E_B is the electron binding energy), the plasmon contribution is transformed into the Compton profile, which reflects the ground-state momentum density of the valence electrons [101]. Also the core-electron contribution to $S(\mathbf{q}, \omega)$, x-ray Raman scattering, transforms to Compton scattering at large q and ω. Both the plasmon regime and the Compton scattering regime are studied to gain insight into the electronic structure of matter [47, 101]. In the intermediate q-region, where the plasmon excitation is damped while the impulse approximation of Compton scattering is not yet valid, electron-hole pair excitations contribute strongly to the spectra leading to complicated behavior [47]. The general behavior of $S(\mathbf{q}, \omega)$ with increasing q can be described as a shift of spectral weight to higher ω ($\omega_{\text{peak}} \sim q^2/2$ based on the f-sum rule [100]) and increased broadening (width $\sim q$ in the Compton scattering regime [101]).

3.3 X-ray Raman scattering

When ω is tuned to a core-electron binding energy, core-electron excitations contribute to $S(\mathbf{q}, \omega)$ in the process called x-ray Raman scattering. In the single-particle excitation picture [99, 102, 103], the dynamic structure factor due to core-electron excitations can be written as

$$S(\mathbf{q}, \omega) = \sum_f \left| \langle f | e^{i\mathbf{q}\cdot\mathbf{r}} | i \rangle \right|^2 \delta(E_f - E_i - \omega), \tag{9}$$

where $|i\rangle$ is a core orbital in the ground state of the system, $|f\rangle$ is a final-state orbital (in the presence of the core hole), and E_i and E_f are the orbital energies. Practical methods for calculating XRS spectra are described in Sec. 5.1–5.2.

The results of XRS are closely connected to x-ray absorption spectroscopy. Expanding the XRS transition operator

$$\exp(i\mathbf{q}\cdot\mathbf{r}) \approx 1 + i\mathbf{q}\cdot\mathbf{r} + \mathcal{O}(q^2) \tag{10}$$

shows that, in the limit of small q, the dynamic structure factor is dominated by dipole transitions $\mathbf{q}\cdot\langle f|\mathbf{r}|i\rangle$. The XRS cross section is then proportional to the XAS cross section (Eq. 2): $S(q \to 0, \omega) \propto \sigma_{\text{XAS}}(\omega)$. This connection has important consequences for practical applications: it allows non-resonant XAS-type studies in cases where the strong resonant absorption would otherwise lead to excessive surface sensitivity and limit measurements to vacuum conditions. The orientational sensitivity of dipole-limit XRS is also related to XAS, with the direction of $\mathbf{q}$ playing the role of the polarization vector $\hat{\mathbf{e}}_1$ [47].

In addition to dipole transitions, XRS also allows probing other transition channels (monopole, quadrupole, ...), with the contribution of non-dipole transitions increasing with q. XRS thus facilitates a rich characterization of the electronic structure in terms of the angular-momentum projected densities of empty states (l-DOS) in the presence of the core hole. This is discussed in more detail in Sec 5.2.

4 Experimental methods

4.1 Synchrotron radiation spectroscopy

Due to the small cross section of NRIXS, and the need for a high relative energy resolution, x-ray sources of very high spectral brightness[2] are required. Synchrotron radiation sources have presented formidable advances in the availability of x-rays of tunable energy and extremely high brightness [104]. The XRS measurements presented in this thesis are only possible at a handful of beamlines with specialized instrumentation (e.g. Refs. 105, 106) in third generation synchrotron sources.

The detection of x-rays is typically based on electronic excitations such as ionization of gases in Geiger counters, photoconversion in scintillation detectors, or electron-hole pair creation in semiconductors [107]. Semiconductor detectors combined with multichannel analyzers enable measuring the energy spectrum of x-rays. The energy resolution of such detectors, however, are limited by the Poisson statistics of the number of generated pairs. For the energy resolution of $\Delta E/E = 10^{-4}$ (1 eV at 10 keV) or better, necessary for studying XRS, the only feasible experimental setups are based on scanning crystal spectrometers [108]. In the following, the multiple-crystal spectrometer at the beamline ID16 of the European Synchrotron Radiation Facility (ESRF) is presented. All the NRIXS experiments in this thesis were performed at ID16.

Beamline ID16 is dedicated to the study of electronic excitations. The detailed layout is presented in paper **I**. X-rays are produced by the ESRF storage ring electrons (current ∼200 mA, energy 6 GeV) in three consecutive undulators (periodic magnetic arrays). The undulator radiation spectrum consist of very bright harmonics, the energy of which can be tuned by varying the undulator gap. The undulator radiation is further monochromatized by a series of crystal monochromators. The first is a high–heat-load LN_2-cooled Si(111) double-crystal monochromator that produces a bandwidth of 1.2 eV at 10 keV. When higher energy resolution is needed, an additional channel-cut monochromator is used to further refine the bandwidth to e.g. 0.2 eV at 10 keV as used in this work to study XRS. The monochromatized radiation can be focused with a Rh-coated toroidal mirror into a spot size of 50×130 μm^2 (V×H). The beamline thus produces a highly monochromatic and focused x-ray beam of high intensity (e.g. 3.5×10^{12} photons/s with a bandwidth of 0.2 eV at 10 keV).

Even with such a high flux, an efficient detection scheme has to be utilized for accurate quantitative XRS studies. At ID16, the scattered x-rays are energy-analyzed and collected by a multiple-crystal spectrometer based on a vertical Rowland-circle geometry [108] (Fig. 2). Nine Si(110) crystal analyzers are housed in a vacuum tank assembly, each spherically bent (bending radius 1 m) to focus the scattered radiation to a detector. The detector is the Maxipix chip [109,110]: a fast-readout photon-counting

[2]defined as the number of photons/s/mm^2/mrad^2/(0.1% bandwidth)

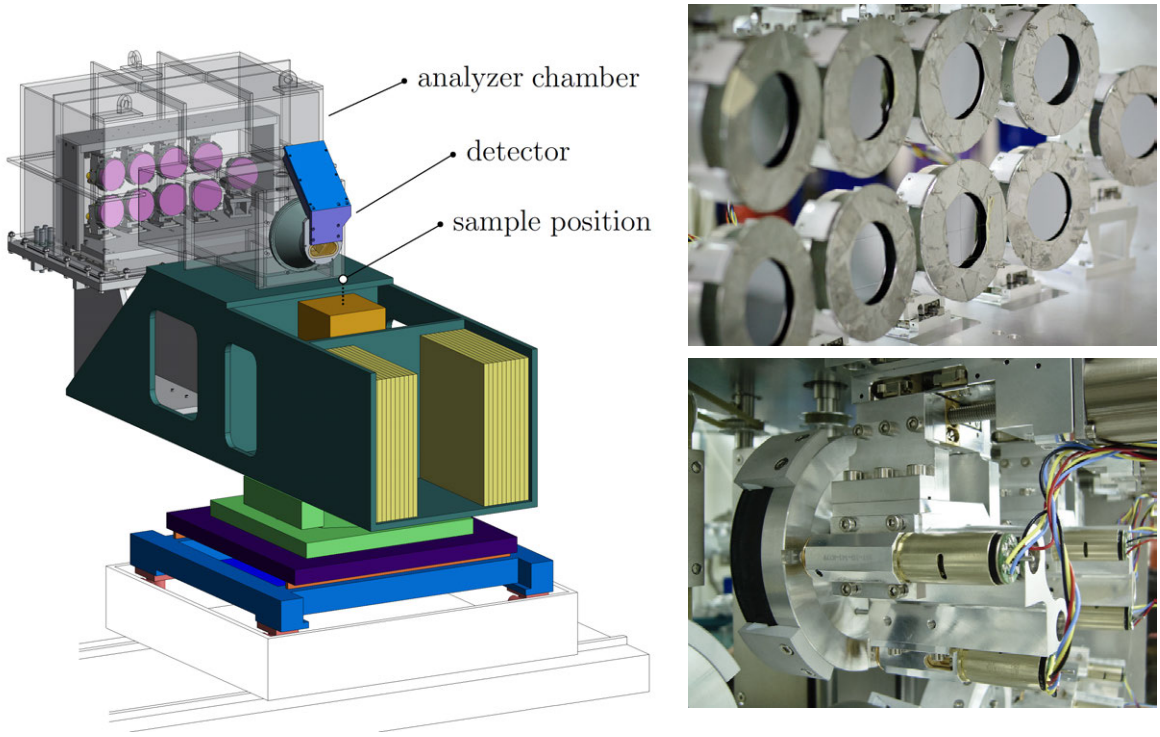

Figure 2: Multianalyzer spectrometer. Left: Schematic of the spectrometer. Top right: Photo of analyzer array. Bottom right: Each analyzer mounting has motors for adjusting orientation and distance from detector.

array of 256×256 pixels, each (55 μm)^2 in size. The combination of spherically bent analyzers and a pixel detector allows the novel application of imaging the origin of the scattered x-rays inside the sample along the beam [111], which was used in this work as an efficient tool for removing background scattering from the sample environment. Contributions to the energy and momentum resolutions are discussed in paper **I**.

4.2 Data analysis

NRIXS spectra are gathered by scanning the incident energy while keeping the analyzer and detector positions fixed, which effectively scans the energy transfer. For small energy transfer ranges (e.g. near-edge studies), the momentum transfer is nearly independent of ω, but for large energy transfer ranges, the variation of q with ω has to be taken into account. In the incident energy scan method, the spectrometer efficiency does not depend on the energy transfer. However, the incident intensity has to be monitored carefully, and any energy dependencies of the monitor efficiency have to be taken into account.

The Maxipix images are stored as separate data files for each exposure, allowing a later software analysis with arbitrary choices of regions-of-interest (Fig. 3). This

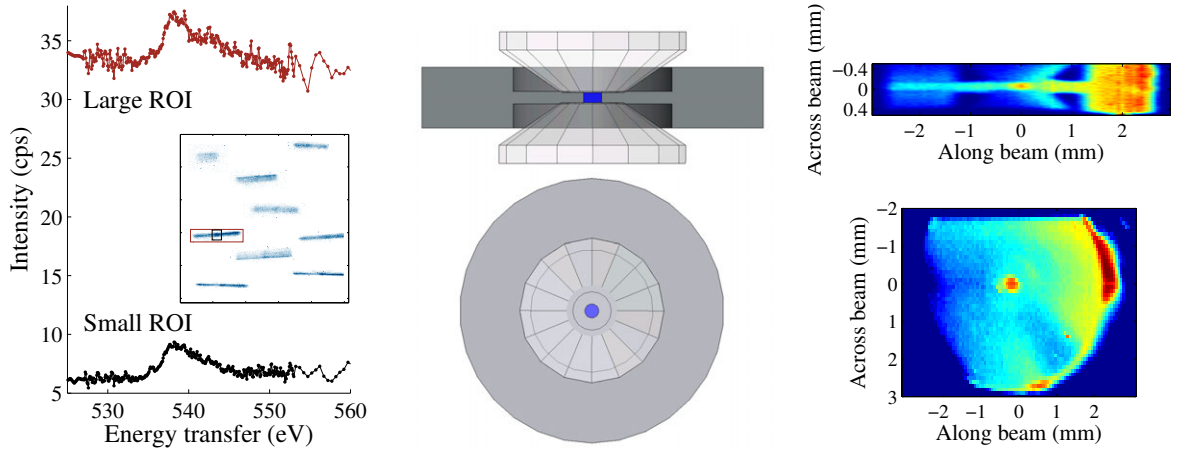

Figure 3: Data analysis. Left: Image on detector with two regions-of-interest (ROI) highlighted, and the resulting spectra from the two ROI. Middle: Schematic cross sections of sample environment (diamond anvil cell). Right: Cross sections obtained by scanning the sample across the beam vertically (top) or horizontally (bottom).

approach is particularly useful in high-pressure experiments where it allows an efficient discrimination of the scattering from the sample environment. It is even possible to do a full tomographic mapping of the sample (with spectroscopic contrast) by scanning the sample across the remaining dimensions [111]. The countrates are divided by the monitor value (corrected for possible energy dependence), and the resulting spectra are then shifted by the individual elastic energy shift of each analyzer and interpolated to a common grid. Various energy-dependent absorption corrections [112] may be necessary to the spectra due to absorption in vacuum windows, the sample environment, or the sample itself.

To separate the XRS contribution from the measured spectra, the background from valence electrons (e.g. plasmon or Compton scattering) needs to be removed. In near-edge studies, the background below the edge is removed by fitting a suitable function to it. For the oxygen K edge at $\omega = 535$ eV, a constant value typically suffices for low-q measurements. For high-q measurements, a pseudo-Voigt function (Pearson VII) is fitted to the sloping valence background below the edge. The spectra could, in principle, be normalized to absolute units (1/eV) with the help of sum rules, e.g. the f-sum rule [47]

$$\int_0^\infty \mathrm{d}\omega\, \omega\, S(q,\omega) = \frac{q^2}{2}. \tag{11}$$

In practice, the spectra are not measured on a large enough energy transfer range, and they are instead usually normalized to equal area with theoretical estimates (Sec. 5.2). Background-corrected and normalized spectra can be inverted to yield the angular-momentum-projected densities of empty states (Sec. 5.2).

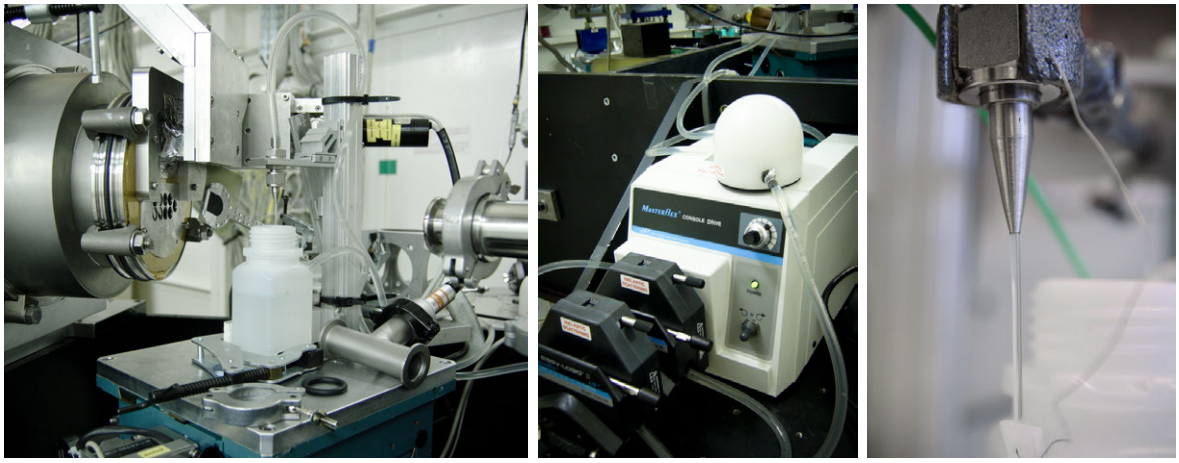

Figure 4: Flow cell for XRS studies of liquids. Left: Setup at the beamline. Middle: Peristaltic pump with dual heads and pulse dampener. Right: Close-up of nozzle and liquid column.

For EXAFS studies, the background removal and signal extraction are more elaborate and involve multiple theoretical and experimental references. XRS analysis in the EXAFS region is studied in detail in paper **V**.

4.3 Sample environments

4.3.1 Flow cell for liquid samples

Due to the small cross section of XRS the samples under study are unavoidably exposed to a large radiation dose. This may be a concern in measurements [113, 114], and it is therefore important to monitor the gathered data for any time-dependent changes. For liquids, these problems can be circumvented by utilizing a liquid exchange system. In this thesis a liquid flow system has been developed that circulates a large volume of liquid and produces a very stable vertical liquid column for measurements. The flow setup was used in papers **II** and **IV**.

The apparatus (Fig. 4) consists of a peristaltic pump with dual heads that pump liquid through two flexible tubes via peristaltic action. The pump heads work in antiphase to reduce the pulsating effect of peristaltic pumps and yield a stable flow. The flow is further stabilized with a pulse-dampening chamber before being directed to a nozzle. The nozzle shapes the flow into a vertical column of 2 mm diameter. Typical flow rates used are 2–3 ml/s yielding a flow velocity of 0.6–1.0 m/s at the nozzle.

The temperature of the liquid can be controlled by incorporating a heat exchanger element into the flow setup. The exchanger is a Cu block with two independent internal circulation channels and an electric heater element. One circulation channel is used for the sample liquid and the other for coolant liquid (e.g. ethanol). The temperature of the

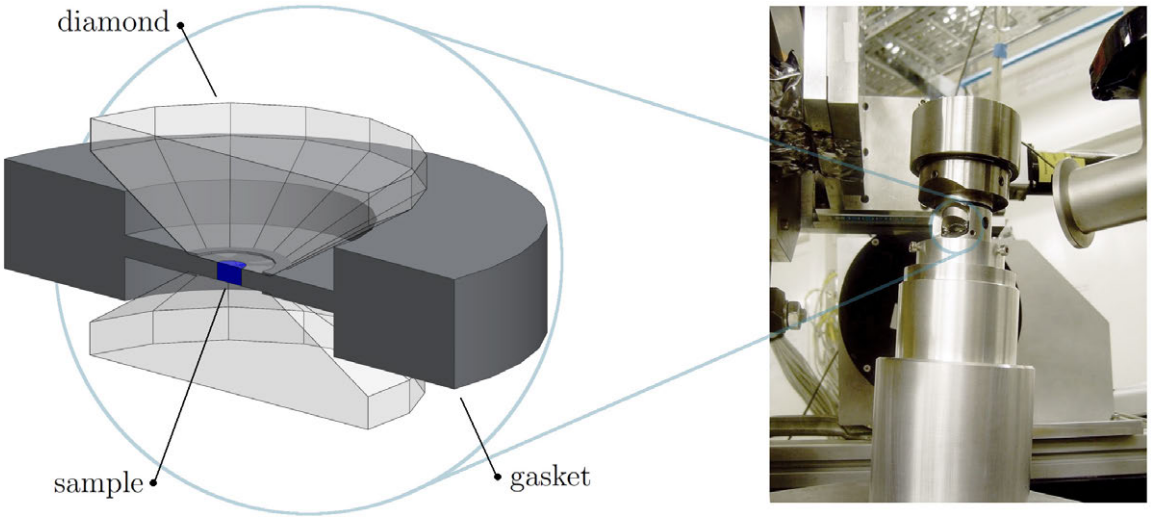

Figure 5: Diamond anvil cell for high-pressure XRS studies. Left: Cross-sectional schematic of a DAC. Right: Panomaric DAC mounted at the beamline.

liquid is adjusted by controlling the power of the heater element with a microcontroller which incorporates a temperature reading from a thermocouple situated in the flow. With this setup, the temperature of liquid water can be stabilized to within 0.1 °C in the range 1.5–86.0 °C.

4.3.2 High-pressure studies with a diamond anvil cell

Pressure is a fundamental thermodynamical parameter that can be adjusted over several orders of magnitude allowing access to a rich variety of phases and phenomena in condensed matter. The diamond anvil cell (DAC) is a versatile high-pressure environment that can reach static pressures of hundreds of GPa, the largest currently achievable [115]. However, DACs are also challenging sample environments as the sample dimensions are typically of the order ∼10–100 μm.

The DAC setup [116] used in paper **III** is shown in Fig. 5. The sample is enclosed inside a metal gasket that is compressed with a pair of small diamonds. The compression is provided by pneumatic loading of a metal membrane. The membrane drives a piston at the end which is one of the diamonds. The small area of the diamond tips (diameter 800 μm) compared to the area of the membrane (diameter several cm) results in the large pressure exerted on the sample. Before loading the cell the diamonds are glued to their baseplates. The relative position and parallelism of the diamond pair are adjusted to a high degree of precision. As the metal gasket also reacts to the compression, several cycles of pre-indentation are necessary before loading the sample.

Whereas most DAC measurements by other techniques are performed through the

diamonds, XRS measurements are typically done with panoramic DACs [67–74]. In a panomaric DAC, the access to the cell is maximized in the gasket plane. Both the incident and scattered x-rays travel through the gasket which allows, with a suitable orientation of the cell, measurements at arbitrary scattering angles. The gasket must be nearly transparent to hard x-rays, and for this reason Be gaskets are used.

In paper **III**, high-pressure phases of ice (denoted ice VI and VII) were produced at room temperature by compressing liquid water to 1.7 and 2.2 GPa, respectively. The pressure inside the DAC was determined by measuring fluorescence from a ruby chip [117] embedded in the sample by means of an optical laser. To produce the transition from ice VII to ice VIII, the DAC setup was cooled by a stream of cryogenic N_2 gas to a temperature of -20 °C. The phases were identified with *in situ* x-ray diffraction.

5 Computational methods

In order to connect structural models with measured spectra, electronic structure calculations [118] are needed. Due to the fast interaction process, core-excited spectra reflect the instantaneous electronic structure of the probed system [99]. Under the Born-Oppenheimer approximation, the instantaneous positions of the nuclei provide the external Coulomb potential for the electrons, whose state is described by the many-particle wave function $|\Psi\rangle$ which is a solution to the Schrödinger equation $\hat{H}|\Psi\rangle = E|\Psi\rangle$.

The full determination of $|\Psi\rangle$ is generally untenable, as it would require solving the many-particle problem. A variety of approximations have been introduced to simplify the situation, often converting the many-particle problem into an effective single-particle problem where the many-particle effects are introduced via an effective potential [100]. In this thesis, two different computational methods are applied to model the spectra as described below.

5.1 Near-edge spectra with density-functional theory

A very powerful simplification of the many-particle problem is provided by density functional theory (DFT) [119,120]. As showed by Hohenberg and Kohn [121], the total energy of a system of interacting electrons is a functional of the electron density $\rho(\mathbf{r})$. Furthermore, there exists a ground-state density, $\rho_{\mathrm{GS}}(\mathbf{r})$, which uniquely minimizes the energy. Other ground-state observables are also, in principle, functionals of the electron density. This simplifies the many-particle problem tremendously: instead of a full description of the N-particle wave function $\Psi(\mathbf{r}_1, \mathbf{r}_2, \ldots, \mathbf{r}_N)$ in a space of $3N$ coordinates (omitting spin for simplicity), it is only necessary to determine the electron

density $\rho(\mathbf{r})$ in 3 dimensions. Unfortunately, the exact density functionals are unknown. However, various approximations of increasing accuracy have been developed.

Kohn and Sham [122] introduced a physically intuitive and computationally efficient approach (KS-DFT) in which the density is constructed with KS orbitals: $\rho(\mathbf{r}) = \sum_i |\phi_i(\mathbf{r})|^2$. Based on DFT, a variational minimization of the total energy leads to the KS equations

$$\Big(-\frac{\nabla^2}{2} + V_{\text{eff}}(\mathbf{r}) \Big) \phi_i(\mathbf{r}) = \epsilon_i \phi_i(\mathbf{r}), \tag{12}$$

where ϵ_i are energy eigenvalues and V_{eff} is the KS potential

$$V_{\text{eff}}(\mathbf{r}) = V_{\text{ext}}(\mathbf{r}) + \int \frac{\rho(\mathbf{r}')}{|\mathbf{r} - \mathbf{r}'|} \, \mathrm{d}\mathbf{r}' + V_{\text{xc}}(\mathbf{r}). \tag{13}$$

The KS equations describe fictitious non-interacting electrons in a potential that includes the external potential of the nuclei (V_{ext}), the mean field due to all the electrons (the Hartree potential), and the exchange-correlation (XC) potential V_{xc}. The XC potential is itself a density functional and contains all many-body effects beyond the Hartree potential. The KS equations can be solved in an iterative, self-consistent manner. In principle, the KS orbitals are only used to construct $\rho(\mathbf{r})$ and have no other physical significance [122]. In practice, the solutions are often used as actual single-particle wave functions [123] so that the many-particle wave function is described as a Slater determinant of the KS orbitals. Furthermore, the KS energies ϵ_i are interpreted as orbital energies and used to calculate excitation energies [124].

In this work KS-DFT was used in the linear combination of atomic orbitals (LCAO) approach to calculate the near-edge XRS spectra of small clusters [125]. This approach has been extensively applied to XAS calculations [88, 89, 92, 95, 126–131]. The spectra are calculated via Eq. 9 using the KS orbitals and their energies. As noted in Sec. 3.3, only the initial core state is a ground-state orbital, and the final states should be calculated in the presence of the core hole. However, by employing Slater's transition state approximation, [99] both the initial and final state can be calculated in the same electronic configuration by inserting half a core hole in the initial state and half an electron in the final state. In practical calculations the final states are kept unoccupied (transition potential approximation, TPA), which allows all the states to be obtained from one calculation [126]. The performance of TPA-DFT for spectral calculations has been discussed extensively [88, 90–92, 95]. It has been shown to produce generally accurate results. However, it may fail in cases where the core-hole interaction is strong [7] (e.g. excitons) and more accurate calculations [93, 94, 132] need to be applied.

The DFT-TPA calculations in papers **II**–**IV** were performed with the StoBe-deMon DFT code [133] which employs Gaussian basis sets and various XC potentials including the local-density approximation (LDA) and different generalized gradient approximations (GGA). The calculations were performed on spherical clusters of 4–6 Å radius with the core-excited atom at the center. The localization of the core hole was ensured

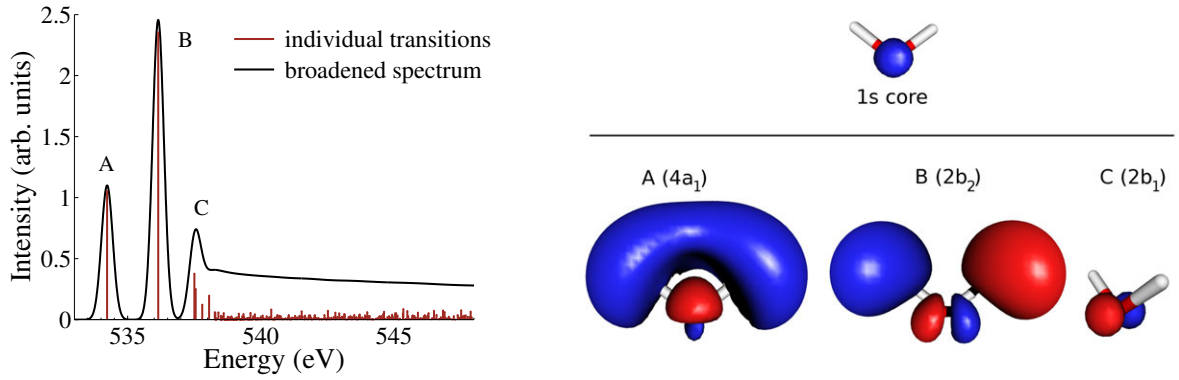

Figure 6: TPA calculation of spectra. Left: Oxygen K-edge dipole-limit spectrum of a water monomer (StoBe calculation). Right: Selected unoccupied KS orbitals corresponding to marked features in the spectrum.

by using pseudopotentials [134] for the core states of other equivalent atoms. Fig. 6 demonstrates how the calculated KS orbitals produce the final spectrum. The calculated spectrum consists of δ-peaks at energies $\epsilon_i - \epsilon_{\text{core}}$, where ϵ_i is the energy of an unoccupied KS orbital and ϵ_{core} is the core orbital energy. The intensities of the peaks follow from Eq. 9. The calculated spectra need to be broadened for comparison with experiment [88]. Various broadening schemes have been presented [88,92]. The typical choice is convoluting each peak with a Gaussian function with an energy-dependent width (Fig. 6).

5.2 Atomic background and momentum transfer dependence

The fundamental feature that separates XRS from other core-excitation spectroscopies is the momentum-transfer dependence, which has been characterized and utilized extensively [47,135–142]. In order to analyze the momentum-transfer dependence of XRS, it is useful to consider the scattering process from a single atom: the core-electron is excited into the continuum as a free spherical wave, leaving behind a core hole. A rigorous method for including the core-hole interaction is to consider the final state as a quasiparticle by introducing a complex self-energy [102, 103]. For energetic photoelectrons, a spherically symmetric atomic potential is a good approximation.

When the atom is no longer isolated the photoelectron final states are perturbed by scattering from the potentials of other atoms. This approach, called real-space multiple scattering (RSMS), can be made exact in the limit of full multiple scattering (FMS). The RSMS allows the very useful separation of the contributions from the central atom and the surroundings, and is the basis for much theoretical and computational work on XAS [102,103,143,144]. Recently, the RSMS code FEFF was extended for calculations of XRS [140].

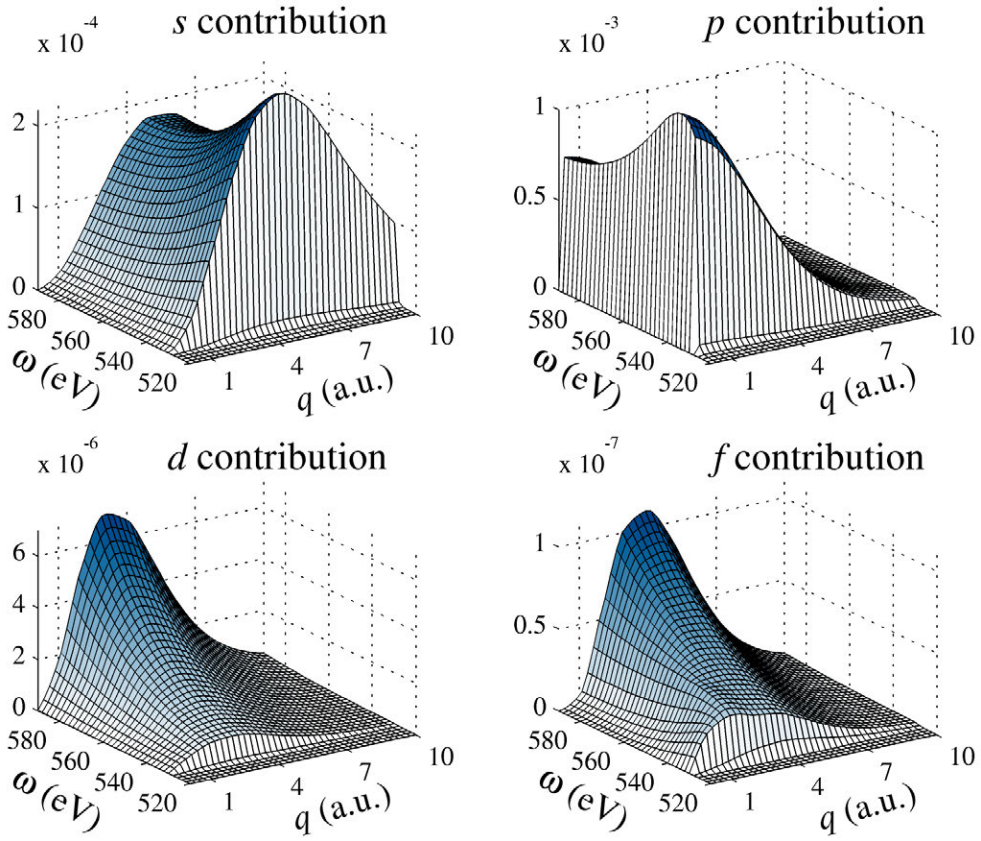

Figure 7: Evolution of matrix elements with momentum transfer: $(2l+1)|M_l(q,\omega)|^2/q^2$ for $l = 0-3$ at the oxygen near-K-edge region (FEFFq calculation of an ice Ih cluster). Note q^{-2} weighting and different scale of each figure.

In the RSMS approach, the final-state density matrix is represented in an angular-momentum and site basis $|L, \mathbf{R}\rangle$ where $L = (l, m)$ [140, 143, 145]. By identifying the term $\sum_f |f\rangle\langle f|\delta(E - E_f)$ in the definition of $S(\mathbf{q}, \omega)$ (Eq. 9) as the density operator, the dynamic structure factor can be written as

$$S(\mathbf{q}, \omega) = \sum_{L,L'} M_L(-\mathbf{q}, E)\rho_{L,L'}(E)M_{L'}(\mathbf{q}, E) \tag{14}$$

where $E = E_i + \omega$, $\rho_{L,L'}(E)$ is the final-state density in $|L, \mathbf{R}\rangle$-basis at the site of the core-excited atom ($\mathbf{R} = 0$), and

$$M_L(\mathbf{q}, E) = \langle L, \mathbf{0}|e^{i\mathbf{q}\cdot\mathbf{r}}|i\rangle \tag{15}$$

are transition matrix elements. The functions $\langle \mathbf{r}|L, \mathbf{0}\rangle = i^l R_l(r)Y_L(\hat{\mathbf{r}})$ are scattering states of the embedded-atom potential and consist of a radial part $R_l(r, E)$ and spherical harmonics $Y_L(\hat{\mathbf{r}})$ [140]. The transition matrix elements $M_L(\mathbf{q}, E)$ depend weakly on the surroundings and are effectively atomic quantities [140, 146]. For isotropic matter

and systems with cubic symmetry, Eq. 14 reduces to

$$S(q,\omega) = \sum_l (2l+1)|M_l(q,E)|^2 \rho_l(E), \tag{16}$$

where $\rho_l(E)$ are the angular-momentum-projected densities of final states (l-DOS). The evolution of $|M_l(q,E)|^2$ is shown for the oxygen near-K-edge region in Fig. 7. The p contribution ($l=1$) peaks at low q, followed by a strong s contribution ($l=0$) at large q. The d and f contributions ($l \geq 2$) are vanishingly small at the near-edge region (note different ordinate axes), but grow rapidly with energy transfer and contribute strongly in the EXAFS region.

Eq. 16 has a very useful application: a measurement of $S(q,\omega)$ at various q-values, combined with calculated matrix elements, allows an inversion of Eq. 16 and thus the experimental determination of the l-DOS [147]. This has been performed in papers **II**–**IV**. The extracted l-DOS may be directly compared to XAS results, e.g. the K-edge XAS signal is proportional to the p-type DOS.

The RSMS approach separates the final-state density operator into contributions from the central atom and the multiple scattering due to the surroundings [102]. This results in a separation of the dynamic structure factor that is similar to what is done in XAS:

$$S(\mathbf{q},\omega) = S_0(q,\omega)\big(1+\chi_{\mathbf{q}}(\omega)\big), \tag{17}$$

where $S_0(q,\omega)$ is the atomic background and $\chi_{\mathbf{q}}(\omega)$ the fine structure [140]. Calculations of $S_0(q,\omega)$ are extremely useful for analyzing and predicting the momentum-transfer dependence of XRS measurements. Representing the effect of neighbors as a fine structure $\chi_{\mathbf{q}}(\omega)$ is the basis of EXAFS analysis; this is considered in the next section.

5.3 Extended fine structure with real-space multiple-scattering approach

In RSMS the effect of neighbors is introduced through photoelectron scattering contributions which modulate the atomic background function [102, 148] via Eq. 17. The modulation can be written as a sum of contributions from multiple-scattering paths j [102, 140, 148]

$$\chi_{\mathbf{q}}(k) = s_0^2 \sum_j \frac{|f_{\text{eff}}^{(j)}(\mathbf{q},k)|}{kR_j^2} \sin\big(2kR_j + 2\delta_c(k) + \phi_{\text{eff}}^{(j)}(\mathbf{q},k)\big) e^{-2R_j/\lambda(k)} e^{-2\sigma_j^2 k^2}, \tag{18}$$

where $k = \sqrt{2E}$ is the photoelectron wave number, R_j is the effective half-path length, $f_{\text{eff}}^{(j)}(\mathbf{q},k) = |f_{\text{eff}}|e^{i\phi_{\text{eff}}}$ is the effective scattering amplitude, and $e^{-2\sigma_j^2 k^2}$ is the Debye-Waller (DW) factor due to thermal motion. Path-independent values include the many-body amplitude reduction factor s_0^2 and the central-atom phase shift δ_c. The path

expansion is limited in R by the photoelectron mean-free path $\lambda(k)$ and the DW factor. Eq. 18 is formally equivalent to the EXAFS equation in XAS [102, 148], but in XRS the effective scattering amplitudes are momentum-transfer dependent [140].

The *ab initio* RSMS code FEFF [140, 143, 144, 149] calculates all the parameters of the EXAFS equation by constructing self-consistent overlapping muffin-tin potentials from atomic densities and uses a complex self-energy [150] for the excited electron. Given a cluster of coordinates, FEFF also enumerates the paths with an efficient sorting algorithm. FEFF produces particularly good results in the EXAFS region (photoelectron energy > 30 eV) where the photoelectron mean-free path limits the expansion to $\sim$10 Å and furthermore the muffin-tin approximation holds well [102]. In the near-edge region FMS calculations may be used, but even then other approximations (e.g. muffin-tin potentials) may fail [102,103]. In this work, FEFF has been used to calculate atomic backgrounds $S_0(q, \omega)$ and transition matrix elements $M_l(q, E)$ in the near-edge region (papers **II**–**IV**), and to calculate $S(q, \omega)$ in the EXAFS region (paper **V**).

6 Summary of papers

In the following five articles are presented which are related to applying x-ray Raman scattering to the study of the structure of disordered matter. Paper **I** presents the technical developments in synchrotron radiation instrumentation that have facilitated the experimental work of this thesis. Papers **II**–**IV** apply the XRS technique to study the effect of H-bonding on the oxygen near-K-edge spectrum in water, high-pressure ices and alcohols. Paper **V** addresses on the application of XRS to measure extended x-ray absorption fine structure, which is experimentally challenging and requires careful data analysis but is very promising for enabling novel applications of EXAFS to light-element systems.

6.1 Paper I: Multiple-element spectrometer for non-resonant inelastic x-ray spectroscopy of electronic excitations

Paper **I** describes the design and commissioning of the new multianalyzer spectrometer at beamline ID16 that was used for all the experimental work of this thesis. The spectrometer is optimized for studying momentum-transfer dependent non-resonant inelastic x-ray scattering in a variety of energy-transfer and momentum-transfer ranges and resolutions. The performance of the spectrometer is shown for both (a) a low-resolution and high-countrate measurement of the dynamic structure factor of polycrystalline diamond in a large range of energy and momentum transfers, and (b) high-resolution measurements of the crystal-field excitations in NiO and acoustic phonons in Al. Various contributions to the momentum and energy resolutions are discussed in detail.

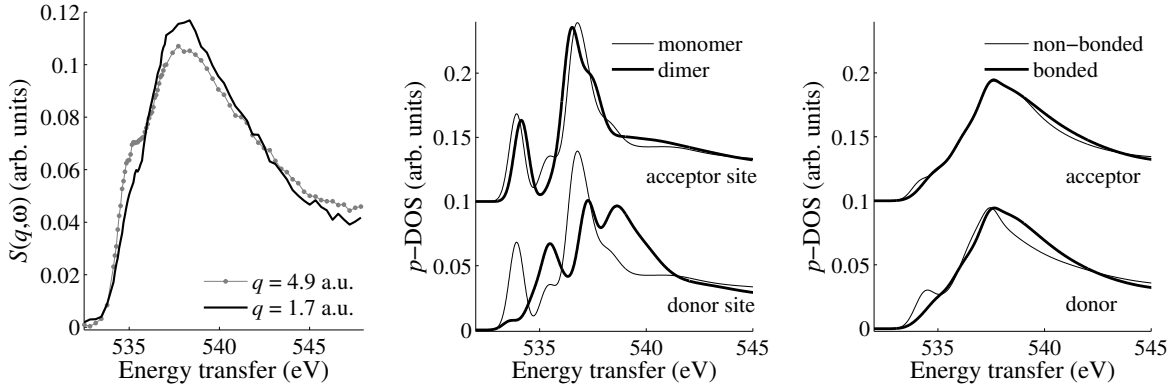

Figure 8: Studying H-bonding in alcohols with XRS. Left: Oxygen K-edge spectra of liquid propanol. Middle: DFT calculations of a propanol dimer and monomer. Right: DFT calculations of MD snapshots of liquid propanol with the central molecule either bonded or non-bonded at the donor/acceptor side.

6.2 Paper II: Universal signature of hydrogen bonding at the oxygen K-edge of alcohols

Core-electron spectroscopies are a novel method for studying H-bonding in disordered matter. Paper **II** presents a systematic study of liquid alcohols using XRS. The samples include the linear alcohols methanol, ethanol, propanol and butanol, as well as the branched isomers isopropanol, isobutanol, and 2-butanol. The experimental spectra are compared with DFT calculations using a large number of MD snapshots and model clusters. The momentum-transfer dependence of the spectrum (Fig. 8) was used to extract the angular-momentum projected DOS.

The calculations of model monomer and dimer clusters clearly indicate that both intra- and intermolecular effects strongly influence the oxygen K-edge spectra. After taking the intramolecular effects into account, however, the effect of H-bonding in the dimer clusters is very similar for all the alcohols. In particular, the selective sensitivity to donor bonds (Fig. 8) is a universal feature. These conclusions remain valid in calculations of realistic MD snapshots. By selectively studying the spectra of snapshots with the core-excited oxygen either bonded or non-bonded, the near-edge spectra are seen to directly reflect the presence of donor HBs in the simulated structures (Fig. 8).

6.3 Paper III: Role of non-hydrogen-bonded molecules in the oxygen K-edge spectrum of ice

Water crystallizes in a large variety of different phases. At least 15 crystalline and three amorphous phases have been characterized. In the crystalline phases the positions of the molecules are well known (apart from proton disorder) [151]. These can thus be

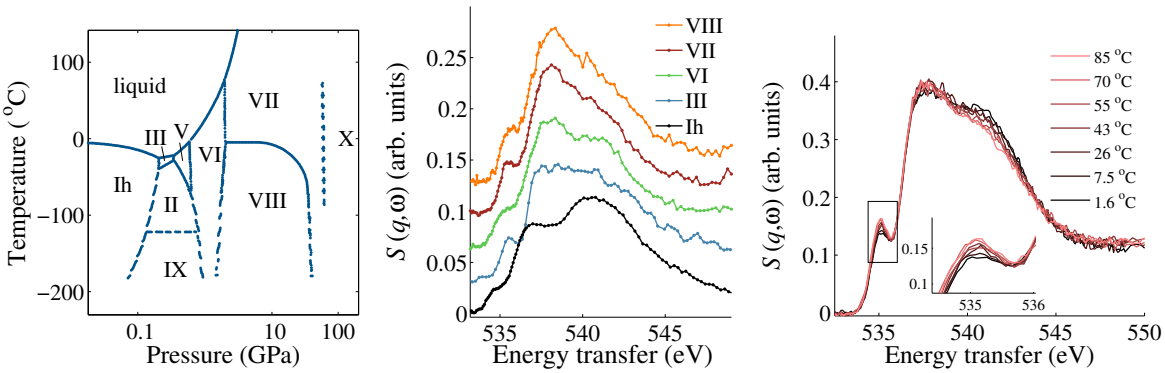

Figure 9: Left: Phase diagram of water with selected high-pressure ice phases [152]. Middle: Oxygen K-edge spectra of high-pressure ices (results offset for clarity). Right: The temperature dependence of the O K-edge in liquid water.

used as model systems for studying the effect of H-bonding on the near-edge spectrum.

These ice phases are challenging to study experimentally. In this paper a diamond anvil cell was used for producing ices VI, VII and VIII. Furthermore, a high-quality single-crystal sample of ice Ih was prepared by the Laboratoire de Glaciologie et Géophysique de l'Environnement (Grenoble, France). The ice phases were chosen to in order to span a large range of densities (from 0.92 to 1.60 g/cm^3) and to include the proton-ordering transition between two similar structures, ice VII and VIII.

The experiments revealed large spectral changes between different ice phases (Fig. 9). This is surprising from the perspective of H-bonding, as the HB geometries change little between these phases. The large density increase results from a contraction of the second coordination shell. In the higher-density ice phases this leads to the formation of two interpenetrating sublattices which form HBs only between themselves. In ices VII and VIII, the non-H-bonded neighbors appear as close as the H-bonded ones. A strong correlation is found for the spectral change in the main- and post-edge region with the average second-shell distance. This is a consistent explanation for the spectral change between these ice phases, and it can also be applied to the spectra of liquid water as well as low and high-density amorphous (LDA and HDA) ices. This is clear evidence that HB formation alone does not explain all the features of the spectrum, and can help explain the discrepancy between traditional structural models and the interpretation of the liquid water spectrum in terms of a large fraction of broken HBs.

6.4 Paper IV: Temperature dependence of the near-edge spectrum of water

The structure of liquid water is still actively discussed. The prevailing view (based on e.g. MD simulations) of a continuous near-tetrahedral local structure [10] is often

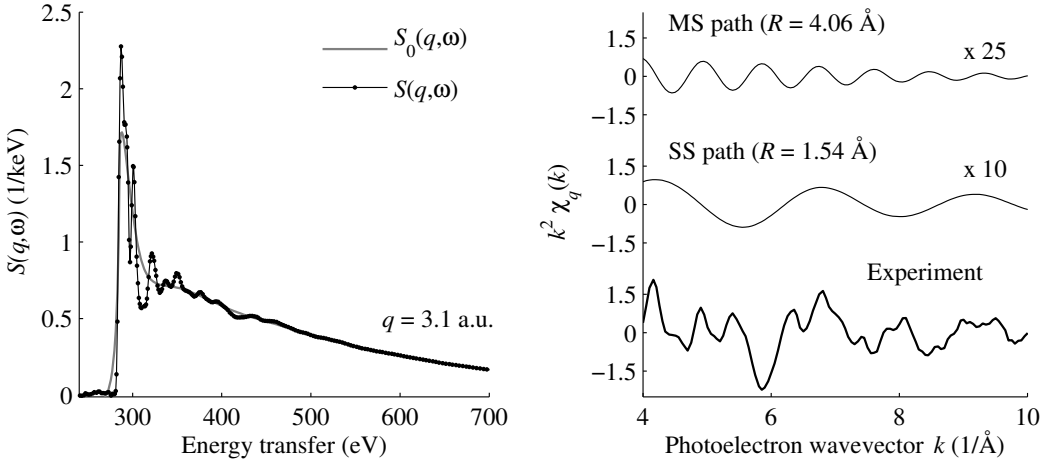

Figure 10: Left: The dynamic structure factor of polycrystalline diamond shows clear EXAFS oscillations at the C K-edge. Right: XRS-EXAFS oscillations extracted from the experiment compared with selected single (SS) and multiple scattering (MS) paths.

challenged by spectroscopic results that are interpreted in terms of mixture models [2, 6,41,43,153]. This interpretation is particularly prevalent in studies of the temperature dependence of the vibrational spectrum [41, 42, 153–155], but has also recently been used to rationalize x-ray absorption and emission results [2, 6, 31, 89].

The temperature evolution of the spectrum (Fig. 9) can be connected to the energetics of those structural rearrangements the that the spectrum is sensitive to. Under the hypothesis of a mixture model, i.e. the existence of two distinct molecular species with different local structures, a van't Hoff analysis [41, 42, 156] can be applied to a selected spectral feature. Since the pre-edge feature has often been connected to broken HBs [2, 3, 31, 129], this was selected and carefully extracted from the measurements. The van't Hoff analysis gives the enthalpy difference ΔH for the conversion between the populations which produce a negligible pre-edge contribution and a strong pre-edge contribution. The small value obtained in the work ($\Delta H = 0.9 \pm 0.2$ kcal/mol) suggests that both populations contributing to the pre-edge would be considered nearly equally H-bonded by energetical criteria. This implies that the pre-edge is sensitive to structural changes which leave HBs intact. The implications of this finding are discussed in detail in the paper.

6.5 Paper V: X-ray Raman scattering based EXAFS beyond the dipole limit

Beyond the near-edge region, XRS spectra exhibit a similar fine structure as EXAFS in x-ray absorption (Fig. 10). This fine structure can be decomposed into contributions from scattering paths from nearest neighbors, providing accurate information on

the local structure (interatomic distances and coordination numbers) even in disordered matter [102, 148]. Whereas EXAFS is routinely studied with x-ray absorption, XRS-EXAFS has only been demonstrated for a handful of systems [82, 157–160]. Experimentally the main challenge is the requirement for extreme statistical accuracy: the oscillating signal dampens as $\sim k^2$ and quickly becomes very challenging to measure. Recent advances in instrumentation have made it possible to also pursue this method with XRS. Another challenge is the interpretation of the spectrum: whereas the analysis of EXAFS is quite routine with modern analysis codes, the momentum-transfer dependence of XRS complicates the situation.

The paper presents a high-quality momentum-transfer-dependent XRS measurement of the EXAFS oscillations of polycrystalline diamond. The data analysis procedure extracts the core-electron contribution from the background due to Compton scattering from valence electrons, and gives a reliable extraction of the oscillations independent of the background shape. This procedure can be readily applied for studying XRS-EXAFS in disordered matter.

A computational analysis of the scattering paths shows that single-scattering paths are insensitive to momentum transfer, but certain multiple-scattering paths change completely. The effect of momentum transfer is visible in the computed real-space signal (Fourier-transformed oscillations). The paper demonstrates both the potential for measuring accurate EXAFS oscillations with XRS, and the need for specialized calculations for analyzing XRS-EXAFS beyond the dipole region.

7 Concluding remarks

Studying the structure of disordered matter with XRS requires the combination of state-of-the-art experimental techniques with various computational approaches. Advances in both fields now allow near-routine studies with XRS. The interpretation of the results, however, remains delicate. The spectral signatures due to bonding changes give indirect information on the local structure that needs to be understood consistently with results from other techniques and MD simulations, taking into account the different specific sensitivity of each technique.

In this thesis the oxygen near-K-edge spectrum has been studied in detail in H-bonded liquids and solids. The sensitivity to HBs have been critically probed. In liquid alcohols the formation of HBs produces a universal spectral signature that is nevertheless influenced by the intramolecular structure. The computed spectra of MD-simulated structures reproduce the room-temperature experimental results very well. The method could be expanded to study H-bonding in alcohols e.g. under supercritical conditions.

For liquid water and ices, new effects have been found which influence the near-edge spectra beyond the breaking of HBs. In particular, the near-edge has been shown to be

sensitive to the non-H-bonded neighbors. Furthermore, the temperature dependence of the liquid water spectrum implies that the pre-edge feature is sensitive to structural changes which leave HBs intact. These novel finding may help resolve some of the conflicting interpretations between diffraction and MD structures on one side and core-excited spectroscopies on the other. With a full understanding of the spectral signatures there is great promise to study a variety of H-bonded systems with the method.

The application of XRS for studying EXAFS oscillations in light-element systems has also been thoroughly assessed with a benchmark measurement of polycrystalline diamond combined with an elaborate data analysis. This work confirms that XRS-EXAFS can be used to expand the EXAFS method to cases where soft x-ray methods are not suitable. These include all light-element absorption edges in bulk samples and embedded in e.g. high-pressure sample environments. In comparing the results with calculations, however, the momentum-transfer dependence should be included in order to model multiple-scattering paths correctly.

The rapid pace of development of IXS instrumentation continues with the introduction of new beamlines and multianalyzer spectrometers. These offer order-of-magnitude improvements in countrates and pave the way for completely new studies, including previously unaccessible sample sizes and timescales, as well as tomographic measurements with spectroscopic contrast.

Related work

List of work by the author that is closely related to this thesis but not included in it:

1. S. Huotari, **T. Pylkkänen**, R. Verbeni, G. Monaco, and K. Hämäläinen. *Direct tomography with chemical-bond contrast.* Nature Materials **10**, 489 (2011).

2. A. Sakko, S. Galambosi, J. Inkinen, **T. Pylkkänen**, M. Hakala, S. Huotari, and K. Hämäläinen. *Inelastic x-ray scattering and vibrational effects at the K-edges of gaseous N_2, N_2O, and CO_2.* Physical Chemistry Chemical Physics **13**, 11678 (2011).

3. S. Huotari, M. Cazzaniga, H.-C. Weissker, **T. Pylkkänen**, H. Müller, L. Reining, G. Onida, and G. Monaco. *Dynamical response function in sodium studied by inelastic x-ray scattering spectroscopy.* Physical Review B (2011), accepted for publication.

4. S. Huotari, J. A. Soininen, **T. Pylkkänen**, K. Hämäläinen, A. Issolah, A. Titov, J. McMinis, J. Kim, K. Esler, D. M. Ceperley, M. Holzmann, and V. Olevano. *Momentum distribution and renormalization factor in sodium and the electron gas.* Physical Review Letters **105**, 086403 (2010).

5. A. Mattila, J. A. Soininen, S. Galambosi, **T. Pylkkänen**, S. Huotari, N. D. Zhigadlo, J. Karpinski, and K. Hämäläinen. *Electron-hole counts in Al-substituted MgB_2 superconductors from x-ray Raman scattering.* Physical Review B **78**, 064517 (2008).

6. S. Huotari, **T. Pylkkänen**, G. Vankó, R. Verbeni, P. Glatzel, and G. Monaco. *Crystal-field excitations in NiO studied with hard x-ray resonant inelastic x-ray scattering at the Ni K edge.* Physical Review B **78**, 041102(R) (2008).

7. A. Mattila, **T. Pylkkänen**, J.-P. Rueff, S. Huotari, G. Vankó, M. Hanfland, M. Lehtinen, and K. Hämäläinen. *Pressure induced magnetic transition in siderite $FeCO_3$ studied by x-ray emission spectroscopy.* Journal of Physics: Condensed Matter **19**, 386306 (2007).

8. K. Nygård, M. Hakala, **T. Pylkkänen**, S. Manninen, T. Buslaps, M. Itou, A. Andrejczuk, Y. Sakurai, M. Odelius, and K. Hämäläinen. *Isotope quantum effects in the electron momentum density of water.* The Journal of Chemical Physics **126**, 154508 (2007).

References

[1] E. D. Isaacs, A. Shukla, P. M. Platzman, D. R. Hamann, B. Barbiellini, and C. A. Tulk, *Covalency of the hydrogen bond in ice: a direct x-ray measurement*, Phys. Rev. Lett. **82**, 600 (1999).

[2] Ph. Wernet, D. Nordlund, U. Bergmann, M. Cavalleri, M. Odelius, H. Ogasawara, L. Å. Näslund, T. K. Hirsch, L. Ojamäe, P. Glatzel, L. G. M. Pettersson, and A. Nilsson, *The structure of the first coordination shell in liquid water*, Science **304**, 995 (2004).

[3] J. D. Smith, C. D. Cappa, K. R. Wilson, B. M. Messer, R. C. Cohen, and R. J. Saykally, *Energetics of hydrogen bond network rearrangements in liquid water*, Science **306**, 851 (2004).

[4] Y. Q. Cai, H.-K. Mao, P. C. Chow, J. S. Tse, Y. Ma, S. Patchkovskii, J. F. Shu, V. Struzhkin, R. J. Hemley, H. Ishii, C. C. Chen, I. Jarrige, C. T. Chen, S. R. Shieh, E. P. Huang, and C. C. Kao, *Ordering of hydrogen bonds in high-pressure low-temperature H_2O*, Phys. Rev. Lett. **94**, 025502 (2005).

[5] K. Nygård, M. Hakala, S. Manninen, M. Itou, Y. Sakurai, and K. Hämäläinen, *Configurational energetics in ice Ih probed by Compton scattering*, Phys. Rev. Lett. **99**, 197401 (2007).

[6] T. Tokushima, Y. Harada, O. Takahashi, Y. Senba, H. Ohashi, L. G. M. Pettersson, A. Nilsson, and S. Shin, *High resolution x-ray emission spectroscopy of liquid water: the observation of two structural motifs*, Chem. Phys. Lett. **460**, 387 (2008).

[7] J. S. Tse, D. M. Shaw, D. D. Klug, S. Patchkovskii, G. Vankó, G. Monaco, and M. Krisch, *X-ray Raman spectroscopic study of water in the condensed phases*, Phys. Rev. Lett. **100**, 095502 (2008).

[8] O. Fuchs, M. Zharnikov, L. Weinhardt, M. Blum, M. Weigand, Y. Zubavichus, M. Bär, F. Maier, J. D. Denlinger, C. Heske, M. Grunze, and E. Umbach, *Isotope and temperature effects in liquid water probed by x-ray absorption and resonant x-ray emission spectroscopy*, Phys. Rev. Lett. **100**, 027801 (2008).

[9] D. Eisenberg and W. Kauzmann, *The Structure and Properties of Water* (Oxford University Press, Oxford, 1969).

[10] F. H. Stillinger, *Water revisited*, Science **209**, 451 (1980).

[11] G. N. I. Clark, C. D. Cappa, J. D. Smith, R. J. Saykally, and T. Head-Gordon, *The structure of ambient water*, Mol. Phys. **108**, 1415 (2010).

[12] T. K. Ghanty, V. N. Staroverov, P. R. Koren, and E. R. Davidson, *Is the hydrogen bond in water dimer and ice covalent?*, J. Am. Chem. Soc. **122**, 1210 (2000).

[13] B. Barbiellini and A. Shukla, *Ab initio calculations of the hydrogen bond*, Phys. Rev. B **66**, 235101 (2002).

[14] T. Head-Gordon and M. E. Johnson, *Tetrahedral structure or chains for liquid water*, Proc. Natl. Acad. Sci. USA **103**, 7973 (2006).

[15] N. E. Cusack, *The Physics of Structurally Disordered Matter* (IOP Publishing, Bristol, 1987).

[16] D. Chandler and J. D. Weeks, *Equilibrium structure of simple liquids*, Phys. Rev. Lett. **25**, 149 (1970).

[17] D. Chandler, *Structures of molecular liquids*, Annu. Rev. Phys. Chem. **29**, 441 (1978).

[18] J. A. Barker and D. Henderson, *What is "liquid"? Understanding the states of matter*, Rev. Mod. Phys. **48**, 587 (1976).

[19] T. Steiner, *The hydrogen bond in the solid state*, Angew. Chem. Int. Ed. **41**, 48 (2002).

[20] O. Mishima and H. E. Stanley, *The relationship between liquid, supercooled and glassy water*, Nature **396**, 329 (1998).

[21] P. G. Debenedetti, *Supercooled and glassy water*, J. Phys.: Condens. Matter **15**, R1669 (2003).

[22] P. Ball, *Water—an enduring mystery*, Nature **452**, 291 (2008).

[23] Y. Marcus, *Effect of ions on the structure of water: structure making and breaking*, Chem. Rev. **109**, 1346 (2009).

[24] P. Ball, *Water as an active constituent in cell biology*, Chem. Rev. **108**, 74 (2008).

[25] K. T. Wikfeldt, M. Leetmaa, A. Mace, A. Nilsson, and L. G. M. Pettersson, *Oxygen-oxygen correlations in liquid water: addressing the discrepancy between diffraction and extended x-ray absorption fine-structure using a novel multiple-data set fitting technique*, J. Chem. Phys. **132**, 104513 (2010).

[26] M. Leetmaa, K. T. Wikfeldt, and L. G. M. Pettersson, *SpecSwap-RMC: a novel reverse Monte Carlo approach using a discrete set of local configurations and pre-computed properties*, J. Phys.: Condens. Matter **22**, 135001 (2010).

[27] A. K. Soper, *An asymmetric model for water structure*, J. Phys.: Condens. Matter **17**, S3273 (2005).

[28] D. T. Bowron, *Experimentally consistent atomistic modeling of bulk and local structure in liquids and disordered materials by empirical potential structure refinement*, Pure Appl. Chem. **80**, 1211 (2008).

[29] T. Head-Gordon and G. Hura, *Water structure from scattering experiments and simulation*, Chem. Rev. **102**, 2651 (2002).

[30] M. Leetmaa, K. T. Wikfeldt, M. P. Ljungberg, M. Odelius, J. Swenson, A. Nilsson, and L. G. M. Pettersson, *Diffraction and IR/Raman data do not prove tetrahedral water*, J. Chem. Phys. **129**, 084502 (2008).

[31] C. Huang, K. T. Wikfeldt, T. Tokushima, D. Nordlund, Y. Harada, U. Bergmann, M. Niebuhr, T. M. Weiss, Y. Horikawa, M. Leetmaa, M. P. Ljungberg, O. Takahashi, A. Lenz, L. Ojamäe, A. P. Lyubartsev, S. Shin, L. G. M. Pettersson, and A. Nilsson, *The inhomogeneous structure of water at ambient conditions*, Proc. Natl. Acad. Sci. USA **106**, 15214 (2009).

[32] A. K. Soper, *Recent water myths*, Pure Appl. Chem. **82**, 1855 (2010).

[33] G. N. I. Clark, G. L. Hura, J. Teixeira, A. K. Soper, and T. Head-Gordon, *Small-angle scattering and the structure of ambient liquid water*, Proc. Natl. Acad. Sci. USA **107**, 14003 (2010).

[34] D. M. Ceperley, *Microscopic simulations in physics*, Rev. Mod. Phys. **71**, S438 (1999).

[35] M. P. Allen and D. J. Tildesley, *Computer Simulation of Liquids* (Oxford University Press, Oxford, 2009).

[36] B. Guillot, *A reappraisal of what we have learnt during three decades of computer simulations on water*, J. Mol. Liq. **101**, 219 (2002).

[37] E. Sanz, C. Vega, J. L. F. Abascal, and L. G. MacDowell, *Phase diagram of water from computer simulation*, Phys. Rev. Lett. **92**, 255701 (2004).

[38] J. R. Errington and P. G. Debenedetti, *Relationship between structural order and the anomalies of liquid water*, Nature **409**, 318 (2001).

[39] R. Iftimie, P. Minary, and M. E. Tuckerman, *Ab initio molecular dynamics: concepts, recent developments, and future trends*, Proc. Natl. Acad. Sci. USA **102**, 6654 (2005).

[40] R. M. Silverstein, G. C. Bassler, and T. C. Morrill, *Spectrometric Identification of Organic Compounds* (John Wiley & Sons, New York, 1991).

[41] W. A. Senior and R. E. Verrall, *Spectroscopic evidence for the mixture model in HOD solutions*, J. Phys. Chem. **73**, 4242 (1969).

[42] G. E. Walrafen, M. R. Fisher, M. S. Hokmabadi, and W.-H. Yang, *Temperature dependence of the low- and high-frequency Raman scattering from liquid water*, J. Chem. Phys. **85**, 6970 (1986).

[43] S. Woutersen, U. Emmerichs, and H. J. Bakker, *Femtosecond mid-IR pump-probe spectroscopy of liquid water: evidence for a two-component structure*, Science **278**, 658 (1997).

[44] J. D. Eaves, J. J. Loparo, C. J. Fecko, S. T. Roberts, A. Tokmakoff, and P. L. Geissler, *Hydrogen bonds in liquid water are broken only fleetingly*, Proc. Natl. Acad. Sci. USA **102**, 13019 (2005).

[45] D. Kraemer, M. L. Cowan, A. Paarmann, N. Huse, E. T. J. Nibbering, T. Elsaesser, and R. J. D. Miller, *Temperature dependence of the two-dimensional infrared spectrum of liquid H_2O*, Proc. Natl. Acad. Sci. USA **105**, 437 (2008).

[46] K. Modig, B. G. Pfrommer, and B. Halle, *Temperature-dependent hydrogen-bond geometry in liquid water*, Phys. Rev. Lett. **90**, 075502 (2003).

[47] W. Schülke, *Electron Dynamics by Inelastic X-Ray Scattering* (Oxford University Press, Oxford, 2007).

[48] M. Hakala, S. Huotari, K. Hämäläinen, S. Manninen, Ph. Wernet, A. Nilsson, and L. G. M. Pettersson, *Compton profiles for water and mixed water-neon clusters: a measure of coordination*, Phys. Rev. B **70**, 125413 (2004).

[49] M. Hakala, K. Nygård, S. Manninen, L. G. M. Pettersson, and K. Hämäläinen, *Intra- and intermolecular effects in the Compton profile of water*, Phys. Rev. B **73**, 035432 (2006).

[50] M. Hakala, K. Nygård, S. Manninen, S. Huotari, T. Buslaps, A. Nilsson, L. G. M. Pettersson, and K. Hämäläinen, *Correlation of hydrogen bond lengths and angles in liquid water based on Compton scattering*, J. Chem. Phys. **125**, 084504 (2006).

[51] K. Nygård, M. Hakala, T. Pylkkänen, S. Manninen, T. Buslaps, M. Itou, A. Andrejczuk, Y. Sakurai, M. Odelius, and K. Hämäläinen, *Isotope quantum effects in the electron momentum density of water*, J. Chem. Phys. **126**, 154508 (2007).

[52] A. H. Romero, P. L. Silvestrelli, and M. Parrinello, *Compton scattering and the character of the hydrogen bond in ice I_h*, J. Chem. Phys. **115**, 115 (2001).

[53] S. Ragot, J.-M. Gillet, and P. J. Becker, *Interpreting Compton anisotropy of ice I_h: a cluster partitioning method*, Phys. Rev. B **65**, 235115 (2002).

[54] C. Bellin, B. Barbiellini, S. Klotz, T. Buslaps, G. Rousse, T. Strässle, and A. Shukla, *Oxygen disorder in ice probed by x-ray Compton scattering*, Phys. Rev. B **83**, 094117 (2011).

[55] K. Nygård, M. Hakala, S. Manninen, K. Hämäläinen, M. Itou, A. Andrejczuk, and Y. Sakurai, *Ion hydration studied by x-ray Compton scattering*, Phys. Rev. B **73**, 024208 (2006).

[56] M. Hakala, K. Nygård, J. Vaara, M. Itou, Y. Sakurai, and K. Hämäläinen, *Charge localization in alcohol isomers studied by Compton scattering*, J. Chem. Phys. **130**, 034506 (2009).

[57] C. Sternemann, S. Huotari, M. Hakala, M. Paulus, M. Volmer, C. Gutt, T. Buslaps, N. Hiraoka, D. D. Klug, K. Hämäläinen, M. Tolan, and J. S. Tse, *Electronic stucture of methane hydrate studied by Compton scattering*, Phys. Rev. B **73**, 195104 (2006).

[58] F. Lehmkühler, A. Sakko, C. Sternemann, M. Hakala, K. Nygård, C. J. Sahle, S. Galambosi, I. Steinke, S. Tiemeyer, A. Nyrow, T. Buslaps, D. Pontoni, M. Tolan, and K. Hämäläinen, *Anomalous energetics in tetrahydrofuran clathrate hydrate revealed by x-ray Compton scattering*, J. Phys. Chem. Lett. **1**, 2832 (2010).

[59] A. Filipponi, *EXAFS for liquids*, J. Phys.: Condens. Matter **13**, R23 (2001).

[60] A. Filipponi, S. De Panfilis, C. Oliva, M. A. Ricci, P. D'Angelo, and D. T. Bowron, *Ion hydration under pressure*, Phys. Rev. Lett. **91**, 165505 (2003).

[61] G. Dalba, P. Fornasini, R. Grisenti, and F. Rocca, *X-ray absorption fine structure: characterization of thermal and structural disorder in non-crystalline solids*, J. Non-Cryst. Solids **345-346**, 7 (2004).

[62] C. Hardacre, *Application of EXAFS to molten salts and ionic liquid technology*, Annu. Rev. Mater. Res. **35**, 29 (2005).

[63] M. Odelius, *Molecular dynamics simulations of fine structure in oxygen K-edge x-ray emission spectra of liquid water and ice*, Phys. Rev. B **79**, 144204 (2009).

[64] P. J. Merkling, A. Muñoz Páez, R. R. Pappalardo, and E. Sánchez Marcos, *Combination of XANES spectroscopy and molecular dynamics to probe the local structure in disordered systems*, Phys. Rev. B **64**, 092201 (2001).

[65] O. M. Roscioni, P. D'Angelo, G. Chillemi, S. Della Longa, and M. Benfatto, *Quantitative analysis of XANES spectra of disordered systems based on molecular dynamics*, J. Synchrotron Rad. **12**, 75 (2005).

[66] J.-P. Rueff and A. Shukla, *Inelastic x-ray scattering by electronic excitations under high pressure*, Rev. Mod. Phys. **82**, 847 (2010).

[67] S. K. Lee, P. J. Eng, H.-K. Mao, Y. Meng, M. Newville, M. Y. Hu, and J. Shu, *Probing of bonding changes in B_2O_3 glasses at high pressure with inelastic x-ray scattering*, Nature Mater. **4**, 851 (2005).

[68] S. K. Lee, P. J. Eng, H.-K. Mao, Y. Meng, and J. Shu, *Structure of alkali borate glasses at high pressure: B and Li K-edge inelastic x-ray scattering study*, Phys. Rev. Lett. **98**, 105502 (2007).

[69] S. K. Lee, J.-F. Lin, Y. Q. Cai, N. Hiraoka, P. J. Eng, T. Okuchi, H.-K. Mao, Y. Meng, M. Y. Hu, P. Chow, J. Shu, B. Li, H. Fukui, B. H. Lee, H. N. Kim, and C.-S. Yoo, *X-ray Raman scattering study of $MgSiO_3$ glass at high pressure: implication for triclustered $MgSiO_3$ melt in Earth's mantle*, Proc. Natl. Acad. Sci. USA **105**, 7925 (2008).

[70] J.-F. Lin, H. Fukui, D. Prendergast, T. Okuchi, Y. Q. Cai, N. Hiraoka, C.-S. Yoo, A. Trave, P. Eng, M. Y. Hu, and P. Chow, *Electronic bonding transition in compressed SiO_2 glass*, Phys. Rev. B **75**, 012201 (2007).

[71] W. L. Mao, H.-K. Mao, P. J. Eng, T. P. Trainor, M. Newville, C.-C. Kao, D. L. Heinz, J. Shu, Y. Meng, and R. J. Hemley, *Bonding changes in compressed superhard graphite*, Science **302**, 425 (2003).

[72] Y. Meng, H.-K. Mao, P. J. Eng, T. P. Trainor, M. Newville, M. Y. Hu, C. Kao, J. Shu, D. Hausermann, and R. J. Hemley, *The formation of sp^3 bonding in compressed BN*, Nature Mater. **3**, 111 (2004).

[73] R. S. Kumar, M. G. Pravica, A. L. Cornelius, M. F. Nicol, M. Y. Hu, and P. C. Chow, *X-ray Raman scattering studies on C_{60} fullerenes and multi-walled carbon nanotubes under pressure*, Diamond Relat. Mater. **16**, 1250 (2007).

[74] M. Pravica, O. Grubor-Urosevic, M. Hu, P. Chow, B. Yulga, and P. Liermann, *X-ray Raman spectroscopic study of benzene at high pressure*, J. Phys. Chem. B **111**, 11635 (2007).

[75] U. Bergmann, O. Mullins, and S. Cramer, *X-ray Raman spectroscopy of carbon in asphaltene: light element characterization with bulk sensitivity*, Anal. Chem. **72**, 2609 (2000).

[76] S. Galambosi, M. Knaapila, J. A. Soininen, K. Nygård, S. Huotari, F. Galbrecht, U. Scherf, A. Monkman, and K. Hämäläinen, *X-ray Raman scattering study of aligned polyfluorene*, Macromolecules **39**, 9261 (2006).

[77] M. Balasubramanian, C. S. Johnson, J. O. Cross, G. T. Seidler, T. T. Fister, E. A. Stern, C. Hamner, and S. O. Mariager, *Fine structure and chemical shifts in nonresonant inelastic x-ray scattering from Li-intercalated graphite*, Appl. Phys. Lett. **91**, 031904 (2007).

[78] T. T. Fister, F. D. Vila, G. T. Seidler, L. Svec, J. C. Linehan, and J. O. Cross, *Local electronic structure of dicarba-closo-dodecarboranes* $C_2B_{10}H_{12}$, J. Am. Chem. Soc. **130**, 925 (2008).

[79] T. T. Fister, G. T. Seidler, E. L. Shirley, F. D. Vila, J. J. Rehr, K. P. Nagle, J. C. Linehan, and J. O. Cross, *The local electronic structure of* α*-*Li_3N, J. Chem. Phys. **129**, 044702 (2008).

[80] A. Sakko, C. Sternemann, C. J. Sahle, H. Sternemann, O. M. Feroughi, H. Conrad, F. Djurabekova, A. Hohl, G. T. Seidler, M. Tolan, and K. Hämäläinen, *Suboxide interface in disproportionating* α*-SiO studied by x-ray Raman scattering*, Phys. Rev. B **81**, 205317 (2010).

[81] H. Conrad, F. Lehmkühler, C. Sternemann, A. Sakko, D. Paschek, L. Simonelli, S. Huotari, O. Feroughi, M. Tolan, and K. Hämäläinen, *Tetrahydrofuran clathrate hydrate formation*, Phys. Rev. Lett. **103**, 218301 (2009).

[82] D. T. Bowron, M. H. Krisch, A. C. Barnes, J. L. Finney, A. Kaprolat, and M. Lorenzen, *X-ray-Raman scattering from the oxygen K-edge in liquid and solid* H_2O, Phys. Rev. B **62**, R9223 (2000).

[83] U. Bergmann, Ph. Wernet, P. Glatzel, M. Cavalleri, L. G. M. Pettersson, A. Nilsson, and S. P. Cramer, *X-ray Raman spectroscopy at the oxygen K-edge of water and ice: implications on local structure models*, Phys. Rev. B **66**, 092107 (2002).

[84] Ph. Wernet, D. Testemale, J.-L. Hazemann, R. Argoud, P. Glatzel, L. G. M. Pettersson, A. Nilsson, and U. Bergmann, *Spectroscopic characterization of microscopic hydrogen-bonding disparities in supercritical water*, J. Chem. Phys. **123**, 154503 (2005).

[85] U. Bergmann, D. Nordlund, Ph. Wernet, M. Odelius, L. G. M. Pettersson, and A. Nilsson, *Isotope effects in liquid water probed by x-ray Raman spectroscopy*, Phys. Rev. B **76**, 024202 (2007).

[86] T. T. Fister, K. P. Nagle, F. D. Vila, G. T. Seidler, C. Hamner, J. O. Cross, and J. J. Rehr, *Intermediate-range order in water ices: nonresonant inelastic x-ray scattering measurements and real-space full multiple scattering calculations*, Phys. Rev. B **79**, 174117 (2009).

[87] A. Nilsson, D. Nordlund, I. Waluyo, N. Huang, H. Ogasawara, S. Kaya, U. Bergmann, L.-Å. Näslund, H. Öström, Ph. Wernet, K. J. Andersson, T. Schiros, and L. G. M. Pettersson, *X-ray absorption spectroscopy and x-ray Raman scattering of water and ice; an experimental view*, J. Electron Spectrosc. Rel. Phenom. **177**, 99 (2010).

[88] M. Leetmaa, M. P. Ljungberg, A. Lyubartsev, A. Nilsson, and L. G. M. Pettersson, *Theoretical approximations to x-ray absorption spectroscopy of liquid water and ice*, J. Electron Spectrosc. Rel. Phenom. **177**, 135 (2010).

[89] M. Odelius, M. Cavalleri, A. Nilsson, and L. G. M. Pettersson, *X-ray absorption spectrum of liquid water from molecular dynamics simulations: asymmetric model*, Phys. Rev. B **73**, 024205 (2006).

[90] B. Hetényi, F. D. Angelis, P. Giannozzi, and R. Car, *Calculation of near-edge x-ray-absorption fine structure at finite temperatures: spectral signatures of hydrogen bond breaking in liquid water*, J. Chem. Phys. **120**, 8632 (2004).

[91] D. Prendergast and G. Galli, *X-ray absorption spectra of water from first principles calculations*, Phys. Rev. Lett. **96**, 215502 (2006).

[92] J. D. Smith, C. D. Cappa, B. M. Messer, W. S. Drisdell, R. C. Cohen, and R. J. Saykally, *Probing the local structure of liquid water by x-ray absorption spectroscopy*, J. Phys. Chem. B **110**, 20038 (2006).

[93] G. Brancato, N. Rega, and V. Barone, *Accurate density functional calculations of near-edge x-ray and optical absorption spectra of liquid water using nonperiodic boundary conditions: the role of self-interaction and long-range effects*, Phys. Rev. Lett. **100**, 107401 (2008).

[94] W. Chen, X. Wu, and R. Car, *X-ray absorption signatures of the molecular environment in water and ice*, Phys. Rev. Lett. **105**, 017802 (2010).

[95] M. Cavalleri, M. Odelius, D. Nordlund, A. Nilsson, and L. G. M. Pettersson, *Half or full core hole in density functional theory x-ray absorption spectrum calculations of water?*, Phys. Chem. Chem. Phys. **7**, 2854 (2005).

[96] M. Leetmaa, M. Ljungberg, H. Ogasawara, M. Odelius, L.-A. Näslund, A. Nilsson, and L. G. M. Pettersson, *Are recent water models obtained by fitting diffraction data consistent with infrared/Raman and x-ray absorption spectra?*, J. Chem. Phys. **125**, 244510 (2006).

[97] M. Weissbluth, *Atoms and Molecules* (Academic Press, Inc., San Diego, 1978).

[98] J. Als-Nielsen and D. McMorrow, *Elements of Modern X-Ray Physics* (John Wiley & Sons, Chichester, 2001).

[99] J. Stöhr, *NEXAFS Spectroscopy* (Springer-Verlag, Berlin, 1992).

[100] D. Pines and P. Nozières, *The Theory of Quantum Liquids* (W. A. Benjamin, New York, 1966).

[101] M. J. Cooper, P. E. Mijnarends, N. Shiotani, N. Sakai, and A. Bansil, *X-ray Compton Scattering* (Oxford University Press, Oxford, 2004).

[102] J. J. Rehr and R. C. Albers, *Theoretical approaches to x-ray absorption fine structure*, Rev. Mod. Phys. **72**, 621 (2000).

[103] C. R. Natoli, M. Benfatto, S. Della Longa, and K. Hatada, *X-ray absorption spectroscopy: state-of-the-art analysis*, J. Synchrotron Rad. **10**, 26 (2003).

[104] C. R. A. Catlow and G. N. Greaves, *Applications of Synchrotron Radiation* (Blackie, Glasgow, 1990).

[105] Y. Q. Cai, P. Chow, C. C. Chen, H. Ishii, K. L. Tsang, C. C. Kao, K. S. Liang, and C. T. Chen, *Optical design and performance of the Taiwan inelastic x-ray scattering beamline (BL12XU) at SPring-8*, AIP Conf. Proc. **705**, 340 (2004).

[106] T. T. Fister, G. T. Seidler, L. Wharton, A. R. Battle, T. B. Ellis, J. O. Cross, A. T. Macrander, W. T. Elam, T. A. Tyson, and Q. Qian, *Multielement spectrometer for efficient measurement of the momentum transfer dependence of inelastic x-ray scattering*, Rev. Sci. Instrum. **77**, 063901 (2006).

[107] G. F. Knoll, *Radiation Detection and Measurement* (John Wiley & Sons, New York, 1989).

[108] Yu. Shvyd'ko, *X-Ray Optics: High-Energy-Resolution Applications* (Springer-Verlag, Berlin, 2004).

[109] X. Llopart, M. Campbell, R. Dinapoli, D. San Segundo, and E. Pernigotti, *Medipix2: a 64-k pixel readout chip with 55 μm square elements working in single photon counting mode*, IEEE Trans. Nucl. Sci. **49**, 2279 (2002).

[110] C. Ponchut, F. Zontone, and H. Graafsma, *Experimental comparison of pixel detector arrays and CCD-based systems for x-ray area detection on synchrotron beamlines*, IEEE Trans. Nucl. Sci. **52**, 1760 (2005).

[111] S. Huotari, T. Pylkkänen, R. Verbeni, G. Monaco, and K. Hämäläinen, *Direct tomography with chemical-bond contrast*, Nature Mater. **10**, 489 (2011).

[112] H. Sternemann, C. Sternemann, G. T. Seidler, T. T. Fister, A. Sakko, and M. Tolan, *An extraction algorithm for core-level excitations in non-resonant inelastic x-ray scattering spectra*, J. Synchrotron Rad. **15**, 162 (2008).

[113] W. L. Mao, H.-K. Mao, Y. Meng, P. J. Eng, M. Y. Hu, P. Chow, Y. Q. Cai, J. Shu, and R. J. Hemley, *X-ray-induced dissociation of H_2O and formation of an O_2–H_2 alloy at high pressure*, Science **314**, 636 (2006).

[114] C. Laffon, S. Lacombe, F. Bournel, and P. Parent, *Radiation effects in water ice: a near-edge x-ray absorption fine structure study*, J. Chem. Phys. **125**, 204714 (2006).

[115] A. Jayaraman, *Ultrahigh pressures*, Rev. Sci. Instrum. **57**, 1013 (1986).

[116] J. C. Chervin, H. Feret, N. Rey, R. Poloni, D. Machon, S. Le Floch, and A. San Miguel, *PanoramiX: a diamond anvil cell designed for radial x-ray investigations*, Proceedings of the 5^{e} Forum de technologie des hautes pressions. Le Réseau de technologie des hautes pressions du CNRS (2006).

[117] J. C. Chervin, B. Canny, and M. Mancinelli, *Ruby-spheres as pressure gauge for optically transparent high pressure cells*, High Pressure Res. **21**, 305 (2001).

[118] R. M. Martin, *Electronic Structure: Basic Theory and Practical Methods* (Cambridge University Press, Cambridge, 2004).

[119] W. Kohn, *Electronic structure of matter—wave functions and density functionals*, Rev. Mod. Phys. **71**, 1253 (1999).

[120] R. G. Parr and W. Yang, *Density-Functional Theory of Atoms and Molecules* (Oxford University Press, Oxford, 1989).

[121] P. Hohenberg and W. Kohn, *Inhomogeneous electron gas*, Phys. Rev. **136**, B864 (1964).

[122] W. Kohn and L. J. Sham, *Self-consistent equations including exchange and correlation effects*, Phys. Rev. **140**, A1133 (1965).

[123] R. Stowasser and R. Hoffmann, *What do the Kohn–Sham orbitals and eigenvalues mean?*, J. Am. Chem. Soc. **121**, 3414 (1999).

[124] A. Savin, C. J. Umrigar, and X. Gonze, *Relationship of Kohn-Sham eigenvalues to excitation energies*, Chem. Phys. Lett **288**, 391 (1998).

[125] A. Sakko, M. Hakala, J. A. Soininen, and K. Hämäläinen, *Density functional study of x-ray Raman scattering from aromatic hydrocarbons and polyfluorene*, Phys. Rev. B **76**, 205115 (2007).

[126] L. Triguero, L. G. M. Pettersson, and H. Ågren, *Calculations of near-edge x-ray-absorption spectra of gas-phase and chemisorbed molecules by means of density-functional and transition-potential theory*, Phys. Rev. B **58**, 8097 (1998).

[127] M. Nyberg, Y. Luo, L. Triguero, L. G. M. Pettersson, and H. Ågren, *Core-hole effects in x-ray-absorption spectra of fullerenes*, Phys. Rev. B **60**, 7956 (1999).

[128] H. Öström, L. Triguero, M. Nyberg, H. Ogasawara, L. G. M. Pettersson, and A. Nilsson, *Bonding of saturated hydrocarbons to metal surfaces*, Phys. Rev. Lett. **91**, 046102 (2003).

[129] S. Myneni, Y. Luo, L. Å. Näslund, M. Cavalleri, L. Ojamäe, H. Ogasawara, A. Pelmenschikov, Ph. Wernet, Z. Västerlein, L. G. M. Pettersson, and A. Nilsson, *Spectroscopic probing of local hydrogen-bonding structures in liquid water*, J. Phys.: Condens. Matter **14**, L213 (2002).

[130] M. Nyberg, M. Odelius, A. Nilsson, and L. G. M. Pettersson, *Hydrogen bonding between adsorbed deprotonated glycine molecules on Cu(110)*, J. Chem. Phys. **119**, 12577 (2003).

[131] A. Nilsson, H. Ogasawara, M. Cavalleri, D. Nordlund, M. Nyberg, Ph. Wernet, and L. G. M. Pettersson, *The hydrogen bond in ice probed by soft x-ray spectroscopy and density functional theory*, J. Chem. Phys. **122**, 154505 (2005).

[132] J. Vinson, J. J. Rehr, J. J. Kas, and E. L. Shirley, *Bethe-Salpeter equation calculations of core excitation spectra*, Phys. Rev. B **83**, 115106 (2011).

[133] K. Hermann, L. G. M. Pettersson, M. E. Casida, C. Daul, A. Goursot, A. Koester, E. Proynov, A. St-Amant, and D. R. Salahub, STOBE-DEMON version 3.0, 2009.

[134] L. G. M. Pettersson, U. Wahlgren, and O. Gropen, *Effective core potential parameters for first- and second-row atoms*, J. Chem. Phys. **86**, 2176 (1988).

[135] S. Doniach, P. M. Platzman, and J. T. Yue, *X-ray Raman scattering in metals*, Phys. Rev. B **4**, 3345 (1971).

[136] M. H. Krisch, F. Sette, C. Masciovecchio, and R. Verbeni, *Momentum transfer dependence of inelastic x-ray scattering from the Li K edge*, Phys. Rev. Lett. **78**, 2843 (1997).

[137] S. Galambosi, J. A. Soininen, K. Hämäläinen, E. L. Shirley, and C.-C. Kao, *Nonresonant inelastic x-ray scattering study of cubic boron nitride*, Phys. Rev. B **64**, 024102 (2001).

[138] K. Hämäläinen, S. Galambosi, J. A. Soininen, E. L. Shirley, J.-P. Rueff, and A. Shukla, *Momentum dependence of fluorine K-edge core exciton in LiF*, Phys. Rev. B **65**, 155111 (2002).

[139] C. Sternemann, M. Volmer, J. A. Soininen, H. Nagasawa, M. Paulus, H. Enkisch, G. Schmidt, M. Tolan, and W. Schülke, *Momentum-transfer dependence of x-ray Raman scattering at the Be K-edge*, Phys. Rev. B **68**, 035111 (2003).

[140] J. A. Soininen, A. L. Ankudinov, and J. J. Rehr, *Inelastic scattering from core electrons: a multiple scattering approach*, Phys. Rev. B **72**, 045136 (2005).

[141] M. W. Haverkort, A. Tanaka, L. H. Tjeng, and G. A. Sawatzky, *Nonresonant inelastic x-ray scattering involving excitonic excitations: the examples of NiO and CoO*, Phys. Rev. Lett. **99**, 257401 (2007).

[142] K. P. Nagle, G. T. Seidler, E. L. Shirley, T. T. Fister, J. A. Bradley, and F. C. Brown, *Final-state symmetry of Na 1s core-shell excitons in NaCl and NaF*, Phys. Rev. B **80**, 045105 (2009).

[143] J. Mustre de Leon, J. J. Rehr, S. I. Zabinsky, and R. C. Albers, *Ab initio curved-wave x-ray-absorption fine structure*, Phys. Rev. B **44**, 4146 (1991).

[144] A. L. Ankudinov, B. Ravel, J. J. Rehr, and S. D. Conradson, *Real-space multiple-scattering calculation and interpretation of x-ray-absorption near-edge structure*, Phys. Rev. B **58**, 7565 (1998).

[145] W. H. Butler, A. Gonis, and X.-G. Zhang, *Multiple-scattering theory for space-filling cell potentials*, Phys. Rev. B **45**, 11527 (1992).

[146] J. J. Rehr, C. H. Booth, F. Bridges, and S. I. Zabinsky, *X-ray-absorption fine structure in embedded atoms*, Phys. Rev. B **49**, 12347 (1994).

[147] J. A. Soininen, A. Mattila, J. J. Rehr, S. Galambosi, and K. Hämäläinen, *Experimental determination of the core-excited electron density of states*, J. Phys.: Condens. Matter **18**, 7327 (2006).

[148] P. A. Lee and J. B. Pendry, *Theory of the extended x-ray absorption fine structure*, Phys. Rev. B **11**, 2795 (1975).

[149] S. I. Zabinsky, J. J. Rehr, A. Ankudinov, R. C. Albers, and M. J. Eller, *Multiple-scattering calculations of x-ray-absorption spectra*, Phys. Rev. B **52**, 2995 (1995).

[150] L. Hedin and B. I. Lundqvist, *Explicit local exchange-correlation potentials*, J. Phys. C **4**, 2064 (1971).

[151] V. F. Petrenko and R. W. Whitworth, *Physics of Ice* (Oxford University Press, Oxford, 1999).

[152] D. D. Klug, *Dense ice in detail*, Nature **420**, 749 (2002).

[153] G. E. Walrafen, *Raman spectral studies of water structure*, J. Chem. Phys. **40**, 3249 (1964).

[154] B. M. Auer and J. L. Skinner, *IR and Raman spectra of liquid water: theory and interpretation*, J. Chem. Phys. **128**, 224511 (2008).

[155] M. Paolantoni, N. F. Lago, M. Albertí, and A. Laganà, *Tetrahedral ordering in water: Raman profiles and their temperature dependence*, J. Phys. Chem. A **113**, 15100 (2009).

[156] G. E. Walrafen, *Effects of equilibrium H-bond distance and angle changes on Raman intensities from water*, J. Chem. Phys. **120**, 4868 (2004).

[157] K. Tohji and Y. Udagawa, *Novel approach for structure analysis by x-ray Raman scattering*, Phys. Rev. B **36**, 9410 (1987).

[158] K. Tohji and Y. Udagawa, *X-ray Raman scattering as a substitute for soft-x-ray extended x-ray-absorption fine structure*, Phys. Rev. B **39**, 7590 (1989).

[159] T. T. Fister, G. T. Seidler, C. Hamner, J. O. Cross, J. A. Soininen, and J. J. Rehr, *Background proportional enhancement of the extended fine structure in nonresonant inelastic x-ray scattering*, Phys. Rev. B **74**, 214117 (2006).

[160] U. Bergmann, A. Di Cicco, Ph. Wernet, E. Principi, P. Glatzel, and A. Nilsson, *Nearest-neighbor oxygen distances in liquid water and ice observed by x-ray Raman based extended x-ray absorption fine structure*, J. Chem. Phys. **127**, 174504 (2007).